Received: 14 September 2025 | Revised: 10 November 2025 | Accepted: 7 December 2025

DOI: 10.1002/alz.71090

Alzheimer's & Dementia®
THE JOURNAL OF THE ALZHEIMER'S ASSOCIATION

RESEARCH ARTICLE

Comprehensive profiling of Aβ40 and Aβ42 fibril-interacting proteins reveals PRKCG as a drug-targetable regulator of amyloidogenesis in Alzheimer's disease

Ana Montero-Calle[1,2] | **Raquel Coronel**[3] | **Juliana Manosalva**[4] | **Diego Megías**[4] | **Vivian de los Ríos**[5] | **Alberto Rábano**[6] | **Alberto Peláez-García**[2] | **Javier Martínez-Useros**[7,8] | **María Jesús Fernández-Aceñero**[9] | **Isabel Liste**[3] | **Rodrigo Barderas**[1,2,10]

[1]Functional Proteomics Unit, Chronic Disease Programme (UFIEC), Instituto de Salud Carlos III, Madrid, Spain

[2]Proteomics Unit (UCCTs), Instituto de Salud Carlos III, Madrid, Spain

[3]Neural Regeneration Unit (UFIEC), Instituto de Salud Carlos III, Madrid, Spain

[4]Advanced Optical Microscopy Unit (UCCTs), Instituto de Salud Carlos III (ISCIII), Madrid, Spain

[5]Centro de Investigaciones Biológicas, CSIC, Madrid, Spain

[6]Alzheimer Disease Research Unit, CIEN Foundation, Queen Sofia Foundation Alzheimer Center, Madrid, Spain

[7]Translational oncology Division, OncoHealth Institute, Health Research Institute-Fundación Jiménez Díaz, Fundación Jiménez Díaz University Hospital/Universidad Autónoma de Madrid (IIS-FJD/UAM), Madrid, Spain

[8]Area of Physiology, Department of Basic Health Sciences, Faculty of Health Sciences, Rey Juan Carlos University, Alcorcón, Madrid, Spain

[9]Surgical Pathology Department, Hospital Universitario Clínico San Carlos, Madrid, Spain

[10]CIBER Frailty and Healthy Aging, Instituto de Salud Carlos III, Madrid, Spain

Correspondence
Ana Montero-Calle, Functional Proteomics Unit, UFIEC, Instituto de Salud Carlos III, E-28220 Majadahonda, Madrid, Spain.
Email: ana.monteroc@isciii.es

Rodrigo Barderas, Functional Proteomics Unit, UFIEC, Instituto de Salud Carlos III, E-28220 Majadahonda, Madrid, Spain.
Email: r.barderasm@isciii.es

Funding information
Ministerio de Educación y Formación Profesional, Grant/Award Number: FPU predoctoral contract; Fundación Tatiana Pérez de Guzmán el Bueno, Grant/Award Number: Predoctoral grant; Ministerio de Ciencia e Innovación, Grant/Award Number: PID2021-126715OB-I00; AES-ISCIII, Grant/Award Numbers: PMP22/00084, PI17CIII/00045

Abstract

INTRODUCTION: Proteins interacting with amyloid beta (Aβ) fibrils could be key to plaque formation in Alzheimer's disease (AD) and represent potential biomarkers and therapeutic targets. Previous proteomic studies using microdissected plaques might have captured non-specific components rather than true Aβ interactors.

METHODS: Biotinylated Aβ40 or Aβ42 peptides were induced to form fibrils, with Scrambled peptides as controls, and incubated with protein extracts from AD and control prefrontal cortex tissue. Pull-down assays coupled with label-free proteomics identified fibril interactors. Dysregulation and localization were assessed by Western blot, immunofluorescence, immunocytochemistry, immunohistochemistry, and in silico analyses.

RESULTS: We identified 185 Aβ40- and 874 Aβ42-associated proteins, with 78 shared. Sixteen proteins, including protein kinase C gamma type (PRKCG), displaying altered

expression in AD, were validated as actual interactors and plaque components *ex vivo*. Remarkably, modulation of PRKCG influenced fibril formation.

DISCUSSION: This study expands the Aβ plaque-associated proteome, identifies novel interactors, and highlights PRKCG as a drug-targetable regulator of AD amyloidogenesis.

KEYWORDS
Alzheimer's disease, amyloid plaques, amyloid beta plaques, Aβ40, Aβ42, biomarkers, label-free, PRKCG, proteomics

Highlights

- A comprehensive proteomic profiling allowed identifying proteins interacting with Aβ40 and Aβ42 fibrils, including many novel interactors.
- Sixteen proteins were validated in vitro and *ex vivo* as bona fide Aβ plaque constituents.
- Dysregulated expression of key interactors was confirmed in AD brain and cell models.
- Modulation of PRKCG activity altered Aβ fibril formation and progression.
- Findings expand the Aβ-associated proteome and highlight novel targets for AD biomarker and therapeutic development.

1 | BACKGROUND

Alzheimer's disease (AD) is the most common form of dementia worldwide, with a rising prevalence and a major social and economic burden.[1] Histopathologically, AD is defined by extracellular amyloid plaques, formed by insoluble amyloid beta (Aβ) aggregates and intracellular neurofibrillary tangles (NFTs) composed of hyperphosphorylated tau protein.[2–5]

Aβ peptides self-assemble into soluble dimers, trimers, oligomers, and insoluble proto-fibrils, which are present in diffuse amyloid plaques and in Aβ halos surrounding dense-core plaques. Over time, they compact into insoluble fibers forming the core of dense-core amyloid plaques (Figure S1a). Deposition follows a sequential pattern, starting in the cortex and spreading to the hippocampus, basal ganglia, thalamus, and basal forebrain, eventually reaching the brainstem and cerebellum.[6]

Amyloid plaques exhibit a heterogeneous composition.[7] The primary constituents of plaques are insoluble forms of the Aβ peptide, resulting from abnormal processing of the amyloid precursor protein (APP), defining key pathological aspects of AD.[7–10] However, plaques also contain other components as extracellular proteins from plasma or cerebrospinal fluid (CSF) – apolipoprotein E (APOE), alpha-1 antitrypsin (SERPINA1), complement factors, or immunoglobulins, intracellular protein components Secernin-1 (SCRN1) or Myelin P2 protein (PMP2), non-protein elements like nucleic acids or lipids, and cellular components.[8,11,12] Cellular components within plaques comprise neurites, reactive microglia, and astrocytes.[13] The characteristic neuritic plaque found in AD patients exhibits a dense core of Aβ fibrils and a less compact ring consisting of tau-positive dystrophic neurites, microglia, and astrogliosis at the periphery, whereas non-compact plaques not associated to glial responses or synaptic loss and composed of aggregates of Aβ proto-fibrils are commonly found in cognitively normal elderly people (Figure S1b).[13]

Importantly, Aβ peptides exhibit variable lengths due to the diverse proteolytic processing of APP. Among the various Aβ peptide species, the most prevalent forms include the 40-amino-acid peptide Aβ(1-40), Aβ40, which represents the most abundant Aβ species in both normal and AD brains, and the 42-amino-acid peptide Aβ(1-42) Aβ42.[14] Both Aβ40 and Aβ42 peptides can form non-fibrillar aggregates, known as Aβ oligomers, and other several aggregate shapes, leading to the development of Aβ amyloid fibrils and plaques.[15–20] Despite being major components of Aβ plaques, it remains unclear which Aβ state is more responsible for AD-associated effects or which peptide is more closely associated with a specific AD subtype. Therefore, understanding not only the structures and biochemical properties of Aβ but also the Aβ40- and Aβ42 plaque-associated proteome is crucial for advances in our comprehension of AD at the molecular level.

Historically, immunohistochemistry (IHC) has been used to identify amyloid plaque-associated proteins. More recently, mass spectrometry-based proteomics has been applied to identify the associated proteome of Aβ plaques through laser capture microdissection (LCM).[21–24] These studies reported roughly 100 enriched proteins but did not reveal clear differences between Aβ40 and Aβ42 plaques.[21] Moreover, plaque heterogeneity and the presence of cellular elements

may confound identification of genuine fibril interactors. Technical limitations also arise from using formalin-fixed paraffin-embedded (FFPE) tissue, which restricts proteome coverage compared to fresh or frozen tissue.[25–28]

In this study, we sought to specifically dissect the proteome associated with Aβ40 and Aβ42 fibrils, avoiding confounding cellular components. We generated biotinylated Aβ40 and Aβ42 fibrils, with Scrambled peptides as controls, and incubated them with protein extracts from prefrontal cortex tissue of AD patients and controls. Pull-down assays followed by in-depth data-dependent acquisition (DDA) label-free quantitative (LFQ) proteomics enabled identifying fibril-binding proteins. Candidate interactors were validated in silico and by WB. Their colocalization with Aβ plaques was assessed *ex vivo* by immunofluorescence (IF) and proximity ligation assay (PLA) on FFPE tissue. Additionally, their dysregulation was further orthogonally evaluated in AD brain tissue and hNS1 neural stem cells and in silico analyses of published proteomics datasets. Among validated interactors, protein kinase C gamma type (PRKCG) was notably downregulated in AD, and functional assays revealed that PRKCG modulation influenced Aβ fibril formation, supporting its role as a regulator of amyloidogenesis.

RESEARCH IN CONTEXT

1. **Systematic review**: Previous proteomic studies of amyloid plaques relied mainly on laser capture microdissection of *post mortem* brain tissue, which may capture non-specific proteins from cellular components rather than true Aβ interactors. No study to date has systematically distinguished between proteins binding to Aβ40 versus Aβ42 fibrils.
2. **Interpretation**: We profiled the fibril interactome of Aβ40 and Aβ42 using biotinylated fibrils and quantitative proteomics, identifying between 185 and 874 interactors, respectively, with 78 shared. Sixteen proteins were validated *ex vivo* as plaque constituents. Among them, PRKCG emerged as a druggable regulator of amyloidogenesis, since its modulation altered Aβ fibril formation.
3. **Future directions**: Our work expands the catalogue of bona fide Aβ fibril-associated proteins and identifies novel candidate biomarkers and targets. Therapeutic strategies aimed at modulating PRKCG or related interactors may help prevent or attenuate amyloid plaque development in AD.

2 | METHODS

2.1 | Tissue samples

The Institutional Ethical Review Board of the Spanish Research Center for Neurological Diseases Foundation (CIEN) and the Instituto de Salud Carlos III approved this study on proteomics analysis and biomarker discovery of Alzheimer's disease (CEI PI 74_2023). Tissue samples with indicated pathological conditions were obtained from the CIEN Foundation's Tissue Bank (BT-CIEN). AD pathology was confirmed after death in all patients.[29] According to the brain bank's protocols, neuropathological diagnosis and classification of cases was performed based on international consensus criteria.[30–32] In all cases, *post mortem* examination was limited to the cranial cavity, according to the brain bank protocol.[29] After fixation, a full neuropathological study was performed in the left half brain by obtaining 25 tissue blocks from cortical and subcortical brain regions.[33] Neuropathological classification of cases was based on the examination of hematoxylin and eosin-stained paraffin sections and immunostaining with a panel of antibodies (Aβ, tau, AT100, α-synuclein, ubiquitin, and transactive response DNA-binding protein 43) and myelin staining. Consensus criteria were used for disease diagnosis and Braak, Thal, and Consortium to Establish a Registry for Alzheimer's Disease staging of AD patients and controls (Table S1 and Table S2). For comparison purposes and stratification of AD patients, Braak stages were used. Alzheimer's histopathological changes were assessed following the National Institute on Aging-Alzheimer's Association (NIA-AA) guidelines.[31] The BT-CIEN developed a brain donation program based on standard operating procedures (SOPs), meeting the ethical and legal requirements established by the current legislation regarding the protection of personal data procedures and the use of samples of human origin for biomedical research. Written informed consent was obtained from all patients.

For the pull-down assays, a total of 18 frozen tissue samples from the left prefrontal cortex of AD patients at Braak V ($n = 6$) and Braak VI ($n = 6$) and from healthy individuals ($n = 6$) were used (Table S1 and Table S2). As the vast majority of proteins identified in AD brain are also found in healthy brains, differing mainly in their relative abundance and post-translational modifications rather than in their presence or absence, the three tissue samples – particularly the two AD cases representing distinct Braak stages – were considered biological replicates for comparative purposes. For the Western blot, a total of 12 frozen tissue samples from the left prefrontal cortex of patients with mild cognitive impairment (MCI, Braak IV [$n = 3$]), from AD patients at Braak V ($n = 3$) and Braak VI ($n = 3$), and from healthy individuals ($n = 3$) were used (Table S1 and Table S2). For IF and PLA, FFPE tissue samples from an AD patient at Braak V ($n = 1$) and from a healthy individual ($n = 1$) were used (Table S1 and Table S2).

2.2 | Cells and immunocytochemistry (ICC)

Immortalized, non-transformed, human fetal forebrain-derived, and multipotent neural stem cells, hNS1 cells were used as a model of AD when APP695 (amyloid precursor protein) was overexpressed. In addition, hNS1 cells without APP overexpression were used as control.[34,35] For APP overexpression, hNS1 cells were infected with lentiviral, and

two different transduced hNS1 subclones were generated: control Φ-eGFP hNS1 cells overexpressing the green fluorescence protein (GFP) and L.APP-IRES-eGFP hNS1 cells overexpressing both human isoform APP695 and GFP proteins. hNS1 cells were grown in a chemically defined human stem cell (HSC) medium (DMEM:F12 containing GlutaMAX [Gibco], 0.6% d-glucose [Merck], 1 × N2 supplement [Gibco], 0.26% AlbuMAX [Gibco], 5 mM HEPES [Gibco], 1 × nonessential amino acids [NEAA; Gibco], 1 × penicillin–streptomycin [Lonza]) supplemented with 20 ng/mL epidermal growth factor (EGF; PeproTech) and 20 ng/mL basic fibroblast growth factor (FGF2; PeproTech). Cells were proliferated on poly-L-lysine (10 µg/mL; Sigma)-coated plastic at 37°C and 5% CO_2. Cells were differentiated by withdrawal of growth factors (EGF and FGF2) and addition of 0.5% heat-inactivated fetal bovine serum (FBS; Gibco) at indicated times.[34]

For ICC, proliferative or differentiated hNS1 cells were rinsed with PBS and fixed for 10 min with 4% paraformaldehyde (PFA, Sigma). Cultures were then blocked for 30 min in 5% normal horse serum (NHS; Gibco) with 0.25% Triton X-100 in PBS (blocking buffer) and incubated O/N at 4°C with the corresponding antibodies (Table S3) diluted in the blocking buffer. Then cells were incubated with an Alexa 555-conjugated donkey anti-rabbit antibody (Invitrogen) for 1 h at RT, and the cell nuclei were counterstained with Hoechst 33,258 (Molecular Probes) at 0.5 µg/mL in PBS for 10 min at room temperature (RT). As negative control, cells were incubated with the Alexa 555-conjugated donkey anti-rabbit IgG, which confirmed the absence of background signal. Fluorescent-immunostained cultures were analyzed in an inverted DMi8 microscope (Leica, Nussloch, Germany). Subsequent fluorescence image analysis was performed using ImageJ after randomly capturing at least seven separate fields per well, with a minimum of three wells per experimental group. The images were converted to 8-bit to quantify the number of positive cells for each antibody in comparison to the total number of cells (Hoechst). A Student's *t*-test was performed, and $p \leq 0.05$ was considered statistically significant.

For PRKCG activation or inhibition, hNS1 CT cells at 4 days of differentiation were incubated either with 1 µM TPPB (Neo Biotech; NB-64-08096) or 50 nM PKC-IN-1 (Neo Biotech; NB-54-03907) for 1 h at 37°C and 5% CO_2. As control, cells were incubated with an equivalent volume of DMSO. Then cells were harvested with 1 mL of lysis buffer (RIPA) supplemented with protease and phosphatase inhibitors to obtain their protein content.

2.3 | Protein extraction

Approximately 100 mg of each frozen left prefrontal tissue sample were cut into small pieces on dry ice and lysed by mechanical disaggregation in 500 µL of lysis buffer (RIPA, Sigma-Aldrich) supplemented with 1× protease and phosphatase inhibitors (MedChemExpress) 1:100 diluted using the TissueLyser II (Qiagen) (two cycles of 30 s at 30 Hz). Then samples were centrifuged at 10,000 × g and 4°C for 10 min and protein extracts (supernatants) collected and stored at −80°C until use. Cell pellets from hNS1 CT or APP cells were lysed in 1 mL of RIPA buffer supplemented with the proteases and phosphatase inhibitors. Pellets were homogenized by repeated passage through 16 and 18 G needles until homogenization were observed, and supernatants with the protein extracts were collected after centrifugation at 10,000 × g and 4°C for 10 min.

Protein concentration was determined with the Trp quantification method and confirmed by Coomassie blue staining after 10% sodium dodecyl sulfate–polyacrylamide gel electrophoresis (SDS-PAGE) under reducing conditions (Figure S2a,cb).[36]

2.4 | Aβ fiber formation

Formation of Aβ fibrils in vitro was induced from biotinylated-Amyloidβ40 (1-40, Anaspec, AS-23512, Aβ40), biotinylated-Amyloidβ42 (1-42, Anaspec, AS-23524, Aβ42), Scrambled-β-Amyloid40 (1-40, Anaspec, AS-24626), and Scrambled-β-Amyloid42 (1-42, Anaspec, AS-25382). First, 0.48 mM Scramble-Amyloid peptides were incubated with 10 mM EZ-Link NHS-Biotin (Thermo Fisher Scientific, 20217) for 30 min at RT and in rotation for biotinylation. Then, for the formation of Aβ fibers, 10 µM of each biotinylated peptide (Scrambled-β-Amyloid40 and Scrambled-β-Amyloid42 as control and Aβ40 and Aβ42 peptides) were incubated separately in PBS 1× in a final volume of 100 µL, at 37°C and 400 rpm for 7 days. Finally, tube contents were fixed with 1% PFA for 30 min at 37°C and stored at −20°C until use.

For the formation of Aβ fibrils after PRKCG activation or inhibition, 10 µM of Aβ40 peptides were incubated with 2 mg of the corresponding protein extract in a final volume of 600 µL with RIPA for 24 h at 37°C and 400 rpm. Aliquots of 60 µL were stored at initial time, 6 h, and 24 h, which were fixed with 1% PFA for 30 min at 37°C and stored at −20°C until use.

Prior to Aβ fiber formation, peptide quality was analyzed by Coomassie blue staining and Western blot after 15% SDS-PAGE, and 2 µg of each biotinylated peptide were analyzed per lane. Transmission electron microscopy (TEM) and confocal microscopy were used for Aβ fiber formation verification.

2.5 | Pull-down assays

Prior to pull-down assays, protein extracts from the left prefrontal cortex brain tissue samples from AD patients at Braak V, Braak VI, and healthy individuals (Table S1 and Table S2) were pooled separately into three groups ($n = 6$). Then 2 mg of each pool were separately preincubated with 20 µL of Streptavidin Mag Sepharose magnetic beads (MBs, Merck, Cytiva 28-9857-38) for 1 h at RT and 25 rpm in a final volume of 300 µL with binding buffer (50 mM Tris, 30 mM NaCl, pH 7.5) to clarify and remove proteins bound non-specifically to MBs.

For the pull-down assays with Aβ fibers, streptavidin MBs were incubated twice with 500 µL of binding buffer for 5 min at RT and 25 rpm for equilibration. Then 0.32 nmol (32 µL) of biotinylated-Aβ40 or biotinylated-Aβ42 fibers or biotinylated-Scrambled-β-Amyloid

(treated as biotinylated-Aβ40 or biotinylated-Aβ42 for fibers formation, but unable to form them) were incubated with 10 µL of MBs per protein extract in separate tubes for 30 min at RT and 25 rpm in a final volume of 300 µL with binding buffer to allow for streptavidin–biotin interaction. Then beads were washed three times with 500 µL of binding buffer for 5 min at RT in rotation and subsequently incubated separately with the previously clarified protein extracts for 2 h at RT and 25 rpm. Finally, MBs were washed three times with 500 µL of binding buffer for 5 min at RT in rotation, and interacting proteins were eluted twice with 50 µL of elution buffer (188 mM Tris pH 6.8, 30% glycerol, 3% SDS, 0.01% bromophenol blue, and 1.5% β-Mercaptoethanol) for 5 min at 95°C and 600 rpm. Finally, 5 µL of eluted proteins were separated using 10% to 15% SDS-PAGE gels for silver staining or to perform WB analysis using appropriate optimized antibody dilutions (Table S3).

2.6 | Transmission electron microscopy

Induced Aβ fibers were analyzed by TEM. To that end, 10 µL of each sample were incubated over glow-discharged carbon-coated grids for 5 min and negatively stained with 2% aqueous uranyl acetate. Then an FEI Tecnai 12 electron microscope equipped with a Lab6 filament operated at 120 kV was used for sample analysis, and images were recorded with the FEI Ceta digital camera.

2.7 | Confocal microscopy

CRANAD-2 staining was performed for visualization of Aβ40 fibers, as previously described.[37] First, glass coverslips (#1.5, Thermo Fisher Scientific) were cleaned by 15-min sonication steps in spectroscopic-grade acetone (PanReac), alkaline detergent (Hellmanex), 0.5 M NaOH solution, and H_2O_{mq} and dried with N_2 prior to incubation with Aβ40 fibers. Then coverslips were incubated with 300 µL of 0.01% poly-L-Lysine (w/v) (Sigma-Aldrich) for 60 min at RT, washed with H_2O_{mq}, dried with N_2, and incubated with 10 µL of Aβ40 fibers in a final volume of 300 µL in PBS 1x for 30 min at RT. Finally, coverslips were washed with H_2Omq and dried with N_2.

Then fibers were incubated with 1:250 dilution in PBS 1× of CRANAD-2 dye (Abcam, 2.5 µg/µL in DMSO) just before image acquisition with an HCX PL APO 100× oil immersion objective (N.A. 1.4) in a Leica Stellaris 8 (STED-Falcon) confocal microscope (Leica Microsystems). For acquisition, a pulse white light laser (Leica Microsystems) was used for excitation at 630 nm and a pulsed laser at 775 nm (40% to 50% laser power) for depletion. A hybrid detector (HyD, Leica Microsystems) with a detection window set to 645 to 730 nm was used with a gate of 0.4 ns with respect to the excitation pulse. Pixel size was set to 16 to 19 nm and the pinhole to 1.0 airy units. Confocal light scanning microscopy (CLSM) and stimulated emission depletion (STED) microscopy images were recorded with unidirectional exposure at 400 Hz using 3× frame average and 1× and 10× line accumulation, respectively. For photobleaching experiments, cumulative STED imaging frames were acquired using 100% depletion laser power every 20 s with a pixel dwell time of 1 µs.

2.8 | LC-MS/MS analysis

25 µL of eluted proteins from the pull-down assays were analyzed by liquid chromatography-tandem mass spectrometry (LC-MS/MS). For trypsin digestion, samples were dried and resuspended in 40 µL of 5% SDS (w/v), reduced with 5 mM Tris (2-carboxyethil) phosphine (TCEP, Thermo Fisher Scientific), and alkylated with 10 mM 2-chloroacetamide (Sigma-Aldrich) for 30 min at 60°C. Then 1:10 diluted 12% phosphoric acid (Sigma-Aldrich, v/v) and 7-fold volumes of binding buffer (90% methanol 100 mM triethylamine bicarbonate [TEAB, Thermo Fisher Scientific]) were added per sample, mixed, and loaded onto an S-Trap filter (Protifi) in two subsequent consecutive steps, separated by a 2-min centrifugation at 3000 × g. Then the filter was washed three times with 150 µL of binding buffer and samples digested. Twenty micrograms of trypsin were diluted in 20 µL of 100 mM TEAB, added to each sample in a relation 1:15 (trypsin:sample), and spun through the S-Trap prior to digestion. Then flow-through was reloaded in the S-Trap column and incubated overnight (O/N) at 37°C in a wet chamber. To avoid leakages from the S-Trap column, a customized yellow tip with 12 Empore 3 M C18 disks (Sigma-Aldrich) was placed at the bottom tip of the S-Trap column during digestion. Peptides were finally eluted by incubating the S-Trap with 40 µL of 25 mM TEAB and with 40 µL of 80% acetonitrile (ACN, Thermo Fisher Scientific) and 0.2% formic acid (FA) for 15 min at RT, separated by a 2 min centrifugation at 3000 × g after each incubation. Eluted peptides were pooled together, dried under vacuum centrifuge, and purified and desalted using OMIX C18 100 µL columns (Agilent Technologies) according to the manufacturer's instructions and dried under vacuum. For analysis by nanosystem LC-MS/MS (nLC–MS/MS), samples were reconstituted in 0.1% FA.

Peptide separation was carried out on an Easy-nLC 1000 nano system (Thermo Fisher Scientific). For the analysis, samples were loaded into a precolumn Acclaim PepMap 100 (Thermo Fisher Scientific) and eluted on an RSLC PepMap C18, 50 cm long, 75 µm inner diameter, and 2 µm particle size (Thermo Fisher Scientific). The mobile phase flow rate was 300 nL/min using 0.1% FA in water (solvent A) and 0.1% FA and 100% ACN (solvent B). The gradient profile was set as follows: 3% to 7% solvent B for 5 min, 7% to 25% solvent B for 95 min, 25% to 60% solvent B for 14 min, 60% to 95% solvent for 1 min, and 95% solvent B for 5 min. Samples were analyzed in triplicate, and 1 µg of each sample was injected per run. MS analysis was performed using a Q Exactive mass spectrometer (Thermo Fisher Scientific).

For ionization, 1900 V of liquid junction voltage and 300°C capillary temperature was used. The full scan method employed a m/z 300 to 1800 mass selection, an Orbitrap resolution of 70,000 (at m/z 200), a target automatic gain control (AGC) value of 3×10^6, and maximum injection time (IT) of 100 ms. After the survey scan, the 15 most intense precursor ions were selected for MS/MS fragmentation. Fragmentation was performed with a normalized collision energy (NCE) of 27 and

MS/MS scans acquired with a starting mass of m/z 200, AGC target of 1×10^5, resolution of 35,000 (at m/z 200), intensity threshold of 2×10^4, isolation window of 1.6 m/z units, and IT of 100 ms. Charge state screening was enabled to reject unassigned, singly charged, and equal or more than seven protonated ions. A dynamic exclusion time of 30 s was used to discriminate against previously selected ions.

2.9 | MS data analysis

MS data were analyzed with MaxQuant (version 1.6.6.0) using standardized workflows. Mass spectra *.raw files were searched against Uniprot UP000005640_9606.fasta Homo sapiens (human) 2021 database (20360 protein entries, downloaded: April 2021) using Reporter ion MS2 type. Trypsin/P was specified as cleavage enzyme, allowing a mass tolerance of 20 ppm (Orbitrap). Precursor and reporter mass tolerance were set to 4.5 ppm and 0.003 Da, respectively, allowing two missed tryptic cleavages. Carbamidomethylation of cysteines was set as a fixed modification, and methionine oxidation, N-terminal acetylation, and Ser, Thr, and Tyr phosphorylation were set as variable modifications. Reporter ion intensities were bias corrected. Unique and Razor peptides were considered for quantification. Minimal peptide length and maximal peptide mass were fixed to seven amino acids and 4600 Da, respectively. Identified peptides were filtered by their precursor intensity fraction with a false discovery rate (FDR) threshold of 0.01. Proteins identified with at least one peptide and an ion score above 99% were considered for evaluation, whereas proteins identified as potential contaminants were excluded from the analysis. The protein sequence coverage was estimated for specific proteins by the percentage of matching amino acids from the identified peptides having confidence greater than or equal to 95% divided by the total number of amino acids in the sequence. Data normalization based on sample loading (SL) was performed with RStudio (version 4.1.1) prior to statistical analysis according to established protocol (https://github.com/pwilmart), using the tidyverse, psych, gridExtra, scales, and ggplot2 packages to equal the total sum of protein intensities per sample (Figure S3a).

For the identification of dysregulated proteins in Aβ40 or Aβ42 samples, Students' *t*-test analysis was performed with RStudio (version 4.1.1) using the dplyr, tidyverse, stats, rstatix, and ggplot2 packages after removal of reverse and contaminant proteins, data filtering (proteins identified in at least 50% samples per group were considered for the analysis), and missing-value imputation by random draws from a gaussian, using the imputeLCMD R package. Adjusted *p* value was obtained applying the Benjamini–Hochberg correction. A FDR ≤ 0.05 was considered statistically significant. Proteins identified with one or more unique peptides, an Aβ/Scrambled ratio ≥ 1.5, and adjusted *p* value ≤ 0.05 were selected as statistically significant dysregulated proteins and, thus, potential interactors of Aβ fibers.

In addition, proteins identified in at least two replicates of the corresponding Aβ samples and identified in no more than one replicate of the corresponding Scrambled samples were considered as specific Aβ40- or Aβ42-interacting proteins in healthy, Braak V, or Braak VI samples.

2.10 | Bioinformatic analysis

Heatmap of the relative abundance of selected proteins were obtained with the pheatmap R package (version 4.4.1) by normalizing to protein intensity. Gene Ontology and Reactome analyses of significantly dysregulated proteins were performed with RStudio (version 4.1.1) using the ReactomePA and biomaRt packages and the Reactome Pathway Database (https://reactome.org/PathwayBrowser, accessed September 21, 2024) to study protein enrichment and to identify the networks and pathways in which Aβ fibers interactors were involved.[38–40] The STRING database was used to elucidate protein–protein interactions previously described among candidate Aβ-interacting proteins (https://string-db.org/cgi/input.pl?sessionId=, accessed September 21, 2024). In addition, the Synaptic Gene Ontologies (synGo 1.1) dataset was used to define the role of dysregulated proteins in the synapse.

2.11 | Western blot

For validation of selected proteins as Aβ fiber interactors, eluted proteins from a second pull-down assay were investigated by WB. Five microliters of each eluted protein sample or 10 µg of each brain protein extract were alternatively separated on 10% or 15% SDS-PAGE under reducing conditions and transferred to nitrocellulose membranes at 100 V for 90 min. Then, membranes were blocked with 0.1% Tween-20 PBS 1× supplemented with 3% bovine serum albumin (BSA) (blocking buffer) for 1 h at RT and incubated with primary antibodies at optimized dilutions (Table S3) in blocking buffer O/N at 4°C and in rotation. Then membranes were washed three times with 0.1% Tween-20 PBS 1× and incubated with the appropriate indicated HRP-conjugated secondary antibodies (Table S3) diluted in blocking buffer for 1 h at RT and in rotation. Next, membranes were washed three times with 0.1% Tween-20 PBS, and, finally, signal was developed using the ECL Pico Plus chemiluminescent reagent (Thermo Fisher Scientific) and detected on an Amersham ImageQuant 800 (Cytiva). Protein band intensities were quantified using ImageJ Software. For brain protein extracts, GAPDH was used as a loading control and for normalization. For pull-down eluted proteins, 4G8 antibody immunostaining was used as a loading control.

2.12 | Immunohistochemistry

The differential expression of potential Aβ interactors was analyzed by IHC using a brain tissue microarray (TMA) containing 37 cores from AD patients at Braak stages IV–VI and healthy individuals as controls with FFPE brain sections of 4 µm. Slides were deparaffinized by incubation at 60°C. Biopsies were cut and incubated with PT-Link (Dako) for 20 min at 95°C in a high pH buffered solution. To block endogenous peroxidase, holders were incubated with peroxidase blocking reagent (Dako). Biopsies were stained for 20 min with the corresponding antibody at optimized dilution (Table S3), followed by incubation with the corresponding HRP-conjugated secondary antibody. Sections were

then visualized with 3,3′-diaminobenzidine for 5 min and counterstained with hematoxylin. Immunoreactivity was graded as 0, absent; 1, mild staining; 2, moderate staining; or 3, intense staining. Cases were classified according to total staining (intensity of the staining per percentage of areas showing reaction). In all cases, an external negative control was included. In addition, TMA incubation with the HRP-conjugated secondary antibody was performed as negative control, which confirmed the absence of background signal. Images at 80× were obtained with the NanoZoomer scanner (Hamamatsu photonics) and processed with NDP.view software.

2.13 | Proximity ligation assay

IF staining was performed using 4-µm FFPE brain tissue sections from an AD patient at Braak stage V ($n = 1$) and a healthy individual ($n = 1$) (Table S1 and Table S2). First, slides were deparaffinized in an oven at 60°C for 30 min and washed for 5 min per wash at RT twice in xylene, twice in 100% ethanol, twice in 96% ethanol, once in 75% ethanol, and once in MilliQ water (H_2Omq). Then slices were incubated with Antigen Retrieval solution (10 mM citrate, pH 6.0) and warmed for 5 min at 120°C and 5 min at 90°C. Slices were then washed for 5 min with Tris-buffered saline, pH 7.6 (TBS 1×), and permeabilized by incubation for 15 min and in rotation with 0.2% Triton X-100 in TBS 1×. Then tissues were washed twice with 0.05% Tween-20 TBS 1× (TBST) for 2 min and in rotation.

Deparaffinized and permeabilized tissues were then immunostained using the tissue protocol of the MolBoolean Mouse/Rabbit kit (Catalog No.: MolB00001) following the manufacturer's instructions. Primary antibodies were diluted in Complete Diluent buffer at corresponding dilutions (Table S3). For immunofluorescence detection, reporters ATTO565 and ATTO647N were used for the detection of Mouse and Rabbit IgGs, respectively. After PLA immunostaining, tissues were incubated with the TrueBlack Lipofuscin autofluorescence quencher (Biotium, ref: 23007) to quench the autofluorescence of lipofusin and tissue sections. Finally, tissues were washed three times with TBS 0.2×, and staining was preserved with Prolong Golf Antifade Mountant (Thermo Fisher Scientific). Images were acquired with an HCX PL APO 63x oil immersion objective (N.A. 1.4) in a Leica Stellaris 8 (STED-Falcon) confocal microscope (Leica Microsystems).

Images were processed with the Leica Confocal software (Las X) and ImageJ. To ensure comparison among images, acquisitions were performed with the same settings (pixel size, excitation laser power, and detector sensitivity). Zoom was adjusted according to the size of the plaques.

2.14 | In silico analysis

The dysregulation of validated Aβ interactors in AD brain tissue samples in comparison with healthy tissue samples was investigated using data from Bai et al. 2020 (PRIDE accession number: PXD007985) and from Montero-Calle et al. 2023 (PRIDE accession number: PXD030751) proteomics experiments.[41,42] Bai et al. analyzed by TMTs LC-MS/MS the protein content from the frontal cortical tissue of large-stage AD patients (AD, $n = 18$) and MCI patients with high Aβ pathology and a slight defect in cognition (MCI, $n = 18$) in comparison with individuals with a low pathology of plaques and tangles (LPC, $n = 18$) and individuals with high Aβ pathology but no detectable cognitive defects (HPC, $n = 18$). Samples were divided into 10 pools (two per pathology) of nine samples per pool. In addition, the researchers analyzed the CSF protein content from LCP ($n = 5$) and AD ($n = 8$) patients. Montero-Calle et al. analyzed the protein content from the left prefrontal cortex tissue samples of AD patients ($n = 12$) in comparison to healthy individuals ($n = 2$) by TMT LC-MS/MS.

For the re-analysis, TMT relative abundance of each pool was averaged, and Students' *t*-test was used for statistical analysis using Microsoft Excel 2019. For the re-analysis of CSF data, signal intensities were averaged for statistical analysis based on a Student's *t*-test two-by-two comparison. Proteins with an AD/Healthy ratio ≥ 1.2 and p value ≤ 0.05 were selected as dysregulated in AD patients.

2.15 | Operetta

Aβ40 aggregates induced in response to PRKCG activation or inhibition were analyzed by fluorescence microscopy using CRANAD-2 dye. First, wells from a 384-well plate were coated with 100 µL of 1:20 Poly-L-Lysine for 1 h at RT. Then, 2 µL of the different Aβ40 aggregates were incubated in 100 µL PBS 1× for 30 min at RT, in duplicate. After incubation, wells were washed twice with 100 µL of H_2Omq and, subsequently, with 100 µL of CRANAD-2 dye diluted 1:250 in PBS 1×, just before image acquisition. Plates were analyzed using the Operetta CLS High-Content Analysis System (Revvity) equipped with a 63× water immersion objective (N.A. 1.5). Images were acquired using an excitation wavelength of 615 to 645 nm and an emission range of 655 to 760 nm. A total of 30 images were captured per well. Image analysis was performed with Harmony software (version 5.2, Revvity) using the PhenoLOGIC machine learning tool, following standard protocols.

2.16 | Statistical analysis

Plots, mean, and standard error of the mean (SEM) of ICC, WBs, and IHC were performed with Microsoft Excel 2019. Student's *t*-test values were calculated with Microsoft Excel 2019. The statistical analysis of proteomics data was performed with R (version 4.1.1). P values ≤ 0.05 were considered statistically significant. A Venn diagram was obtained at the jvenn website (http://bioinfo.genotoul.fr/jvenn).[43]

3 | RESULTS

3.1 | Identification of Aβ-interacting proteins

For the identification of Aβ interactors, commercial biotinylated Aβ40, biotinylated Aβ42, Scrambled-β-Amyloid40 (Sc-β-A40), and Scrambled-β-Amyloid42 (Sc-β-A42) were used. Scrambled commercial

peptides were biotinylated and the quality of Aβ and Scrambled peptides analyzed by Coomassie blue staining and WB prior to further use (Figure S1c). Then, 10 μM of each biotinylated peptide was separately incubated for 7 days at 37°C in PBS and 400 rpm to induce the aggregation and formation of fibrils. Prior to pull-down assays, samples were analyzed to confirm the formation of Aβ fibers by TEM (Figure S1d). As expected, only Aβ40 and Aβ42 peptides were able to form Aβ fibers, in contrast to Scrambled peptides. Moreover, due to the higher trend to aggregate Aβ42 peptides, Aβ42 fibrils formed more dense fiber accumulations than Aβ40 fibers. Finally, the formation of Aβ40 fibers was confirmed by CLSM and STED microscopy after incubation with CRANAD-2 dye, which specifically bind to Aβ40 fibers (Figure S1e). These results, together with the observation that the overall appearance of the biotinylated fibrils (helical twist, continuity, and bundle formation) was consistent with previously reported TEM images of non-biotinlyated Aβ fibrils,[44] suggest that biotinylation did not induce any abnormal conformation in the fibrils.

Next, samples of Aβ40 and Aβ42 fibrils were used for pull-down assays. The Aβ40 and Aβ42 fibrils were immobilized on streptavidin MBs and separately incubated with pooled protein extracts from left prefrontal cortex tissue samples of Braak V ($n = 6$) and Braak VI ($n = 6$) AD patients, as well as healthy individuals ($n = 6$), aimed at the enrichment of the samples on proteins interacting with the Aβ fibrils. The rationale for selecting these samples for the pull-down assays was two-fold. First, Braak V–VI stages represent the most advanced AD neuropathological phase, with fully developed amyloid and tau pathology, thereby increasing the likelihood of capturing stable and disease-relevant Aβ fibril interactors. Second, we included a group of healthy individuals to identify baseline interactions that may occur in the absence of AD pathology. While we hypothesize that at earlier stages – such as Braak I–II (prodromal) or Braak III–IV (MCI) – and control group Aβ interactors might be more transient or present at lower abundance, making their biochemical detection more challenging, the combination of late-stage and control samples would maximize the detection of disease-relevant fibril-associated proteins from baseline interactions (control samples) and those that are enriched in late-stage AD.

Moreover, Sc-β-A40 and Sc-β-A42 samples, obtained from the incubation of Scrambled peptides in PBS, served as negative controls to identify non-specific interacting proteins. Finally, Aβ fiber-interacting proteins were eluted and analyzed prior to LC-MS/MS analysis by silver staining after 10% SDS-PAGE to confirm the isolation of potential Aβ40 or Aβ42 interactors, respectively (Figure S2b).

For the identification of Aβ40 fibril protein interactors, 2126 proteins were identified by LFQ proteomics analyses, with 1948 proteins identified and quantified with one or more unique peptides in more than 50% of the analyzed samples (Table S4). For the LFQ analysis of Aβ42 fibrils, 3265 proteins were identified and 1411 proteins identified and quantified with at least one unique peptide in more than 50% of the analyzed samples per group (Table S5). Additionally, a correct sample clustering was observed in both experiments after principal component analysis, confirming the quality of the proteomics data for the study (Figure S3b).

Then two different analyses were performed for the identification of potential Aβ40 and Aβ42 interactors. First, statistical analysis of Aβ fiber interactors (including eluted proteins from Braak V, Braak VI, and healthy individuals) in comparison with proteins eluted from the pull-down assays with Scrambled peptides (Scrambled analysis) revealed 22 and 69 Aβ40 or Aβ42 potential interacting proteins, respectively, with an Aβ/Scrambled ratio ≥ 1.5 and an adjusted p value (FDR) ≤ 0.05 (Figure 1A, Table S4 and Table S5), with five of these proteins common to Aβ40 and Aβ42 (Figure 1B). Interestingly, among these 85 unique proteins identified as potential Aβ fibril-interacting proteins, APP, and other blood components associated with AD-related vascular pathology were identified, such as fibrinogen gamma chain (FGG) or HBA1/2 (hemoglobin subunits alpha 1/2), pointing to a high quality of the proteomics data obtained. Furthermore, PMP2 was also identified among Aβ42-interacting proteins, which had been previously described as associated with Aβ plaques by *ex vivo* analysis using FFPE brain tissue samples.[42] Second, we focused on the 163 and 806 proteins identified as specific interactors of Aβ40 or Aβ42, respectively (Figure 2A, Table S4, and Table S5), which were not present in the Scrambled samples, with 73 of these proteins being common to Aβ40 and Aβ42 (Figure 2B).

3.2 | Bioinformatic analysis

Next, proteins identified as upregulated in Aβ-induced fibrils (85) or as Aβ40 (90), Aβ42 (373), or Aβ40 and Aβ42 (73) specific proteins were further analyzed to elucidate their role in the disease and in the formation of Aβ plaques using different bioinformatic tools. First, we investigated the biological pathways in which dysregulated and specific proteins were involved, separately, to elucidate any biases related to the nature of the Aβ peptides. Notably, most of these proteins were described in synapses and signaling and involved in processes related to secretion, exocytosis, or cellular organization, transport, and localization (Figures 1C, 2D,E). In addition, Aβ42-specific proteins were also involved in metabolic processes and in Aβ clearance, which can be directly related to the formation of Aβ plaques (Figure 2E). Altogether, these changes resulted in a dysregulation in metabolic, signaling, and response to stimuli processes induced by the production of Aβ40 and Aβ42 peptides and the formation of Aβ plaques (Figure S4a). As most of these proteins were related to synapses, we further investigated their role in this process with the SynGo tool. Dysregulated proteins and Aβ40-specific proteins were mainly presynaptic proteins involved in vesicle cycle and signaling (Figure 1D, Figure 2F). In contrast, Aβ42-specific proteins were related to metabolic, presynaptic, and postsynaptic processes (Figure 2G). Finally, we also investigated previously described protein–protein interactions among candidate dysregulated and common Aβ40- and Aβ42-specific interacting proteins using the STRING tool (Figure S4b). Interestingly, 14 clusters of direct or indirect interactions among candidate Aβ fibril interactors were obtained, with significant associations (FDR ≤ 0.05) related to microtubule organization, oxidative phosphorylation, metabolic processes, protein transport, and signaling pathways. Together, these findings suggest that the dysregulation of

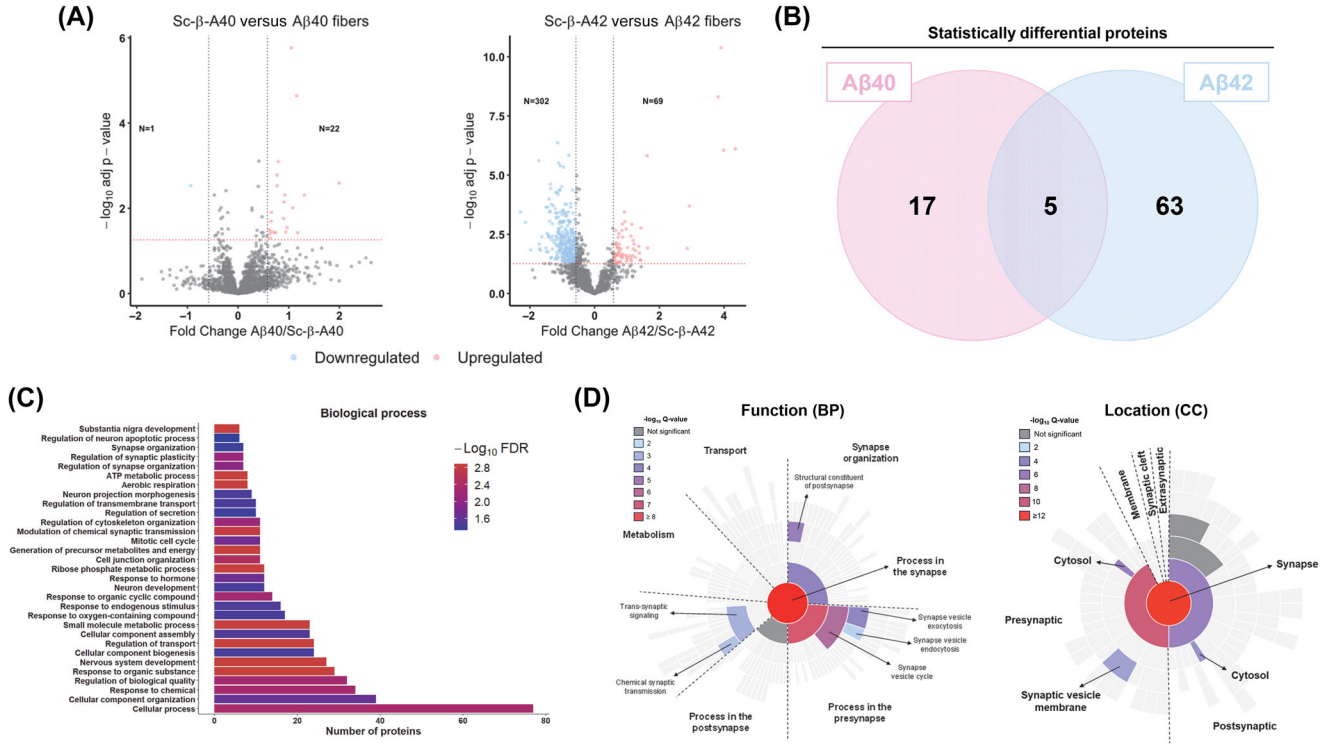

FIGURE 1 Statistical dysregulation analysis of LFQ proteomics of pull-down assays with Aβ40 and Aβ42 fibers. (A) Volcano plots of proteins identified as Aβ40 (left) or Aβ42 (right) significant interactors after Scrambled analysis (ratio Aβ/Scrambled). The *x*-axis is $\log_2$ ratio (fold change) of protein abundance differences between the two groups; the *y*-axis is FDR value (adjusted *p* value) based on $-\log_{10}$. The colored dots represent proteins overrepresented in the Aβ samples (red) and proteins overrepresented in the Scrambled samples (blue) with FDR ≤ 0.05 (FDR = 0.05 represented by a red dashed horizontal line) and 1.5-fold expression difference (represented by two black dashed vertical lines). (B) Venn diagram analysis of potential Aβ-interacting proteins identified in the two LFQ proteomics experiments. Five proteins were identified as common Aβ40 and Aβ42 interactors, whereas 17 and 63 proteins were specifically associated to Aβ40 or Aβ42 fibers, respectively. (C) Enriched biological processes in which dysregulated Aβ interactors are involved were represented after GO analysis. Bar length is proportional to the number of proteins associated with the GO annotation. The statistical significance of each pathway (FDR) is represented in a red-blue scale. (D) SynGo analysis of function (right) and location (right) in synapse of dysregulated proteins. Significant process related to synapse, presynaptic, and postsynaptic processes where dysregulated proteins were involved are depicted ($q < 0.01$). Aβ, amyloid beta; DDA, data-dependent acquisition; FDR, false discovery rate; GO, Gene Ontology; LFQ, label-free quantitative.

these processes and their associated proteins may contribute to the aggregation of Aβ peptides into fibrils and the formation of Aβ plaques. Alternatively, the accumulation of Aβ peptides within cells may disrupt these processes, further contributing to the pathophysiology of AD.

Following bioinformatics analysis, 16 proteins were selected for in vitro and *ex vivo* validation as interacting proteins of Aβ fibers (Table 1). The selection was based on the following criteria: (1) expression ratio, (2) identification as interactors of Aβ40 and/or Aβ42, (3) their biological roles and prior associations with AD, and (4) the availability of reagents for validation.

3.3 | Validation of potential interactors

Among the 16 interactors selected for validation and according to our proteomics results, two were identified as Aβ40 and Aβ42 interactors, three as Aβ40-specific interactors, and 11 as Aβ42-specific interactors (Figure 3A, Table 1). Interestingly, all the Aβ42 interactors were also detected in the Aβ40 samples, albeit with non-significant ratios or FDR values. Similarly, this pattern was observed for the Aβ40 interactors in the Aβ42 samples. To confirm the association of candidate interactors with Aβ, we performed a new pull-down assay with newly synthesized Aβ40, Aβ42, and Scrambled fibrils, and the presence of the 16 proteins selected was investigated by WB (Figure 3B). Additionally, 4G8 immunostaining, used as loading control in the pull-down assays with Aβ40 and Aβ42 fibrils, revealed specific detection of Aβ peptide, indicating that the 4G8-accessible surface epitope was preserved in the biotinylated fibrils. Moreover, together with TEM, CLSM, and STED analyses of Aβ40 and Aβ42 fibrils, these results supported the notion that biotinylation did not induce any abnormal conformation, thereby confirming the validity and specificity of the technique and of the proteomics and pull-down data. First, DNM1, PSD3, and PRKCG and PA2G4 and PSMC4 were validated as Aβ40- or Aβ42-interacting proteins, respectively, and PCCA and PCCB were verified as Aβ40- and Aβ42-interacting proteins. Additionally, SV2A, FSCN1, CDC42, cathepsin B (CTSB), CNRIP1, CLDN11, RHOA, NRGN, and PRNP were found to interact with both Aβ40 and Aβ42 fibrils. These

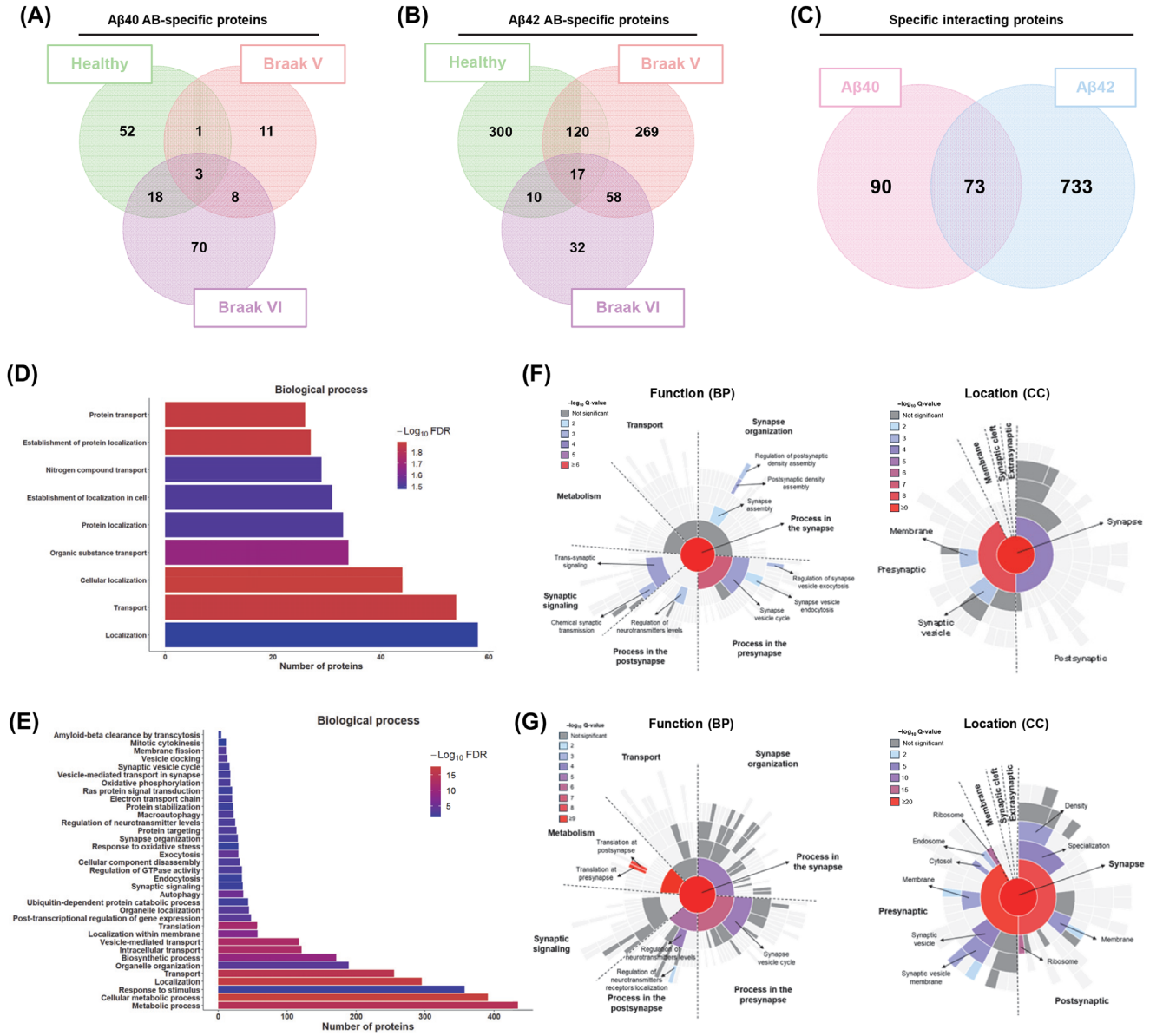

FIGURE 2 Bioinformatics analysis of specific Aβ40- and Aβ42-interacting proteins. (A) Venn diagram specific (A) Aβ40- and (B) Aβ42-interacting proteins identified in healthy, Braak V, and Braak VI samples in comparison to Scrambled samples. (C) Venn diagram analysis of Aβ40- and Aβ42-specific interacting proteins revealed 73 common proteins, and 90 and 732 proteins specific to Aβ40 or Aβ42 fibers. (D) Enriched biological processes in which Aβ40 specific proteins are involved were represented after GO analysis. Bar length is proportional to the number of proteins associated with the GO annotation. The statistical significance of each pathway FDR is represented in a red-blue scale. (E) Enriched biological processes in which Aβ42-specific proteins are involved were represented after GO analysis. Bar length is proportional to the number of proteins associated with the GO annotation. The statistical significance of each pathway (FDR) is represented in a red-blue scale. (F) Enriched biological processes in which Aβ42-specific proteins are involved were represented after GO analysis. Bar length is proportional to the number of proteins associated with the GO annotation. The statistical significance of each pathway (FDR) is represented in a red-blue scale. (G) SynGo analysis of function (right) and location (right) in synapse of Aβ42-specific proteins. Significant processes related to synapse, presynaptic, and postsynaptic processes where dysregulated proteins were involved are depicted ($q < 0.01$). Aβ, amyloid beta; FDR, false discovery rate; GO, Gene Ontology.

results corroborate the previous proteomics data and suggest that most Aβ-interacting proteins can be associated with both Aβ40 and Aβ42 peptides. Moreover, a faint PRKCG band was detected in the pull-down WB of healthy brain tissue extracts incubated with both scAβ40 and Aβ40 fibrils, suggesting a non-specific interaction of PRKCG in healthy samples with Aβ40 fibrils. In contrast, PRKCG interaction with Aβ40 fibrils was shown specific in AD patients, suggesting that post-translational modifications of this protein occurring in AD patients might promote its interaction with Aβ40 fibrils. Furthermore, these findings underscore the significance of these interacting proteins for a better understanding of the disease and their potential as therapeutic targets by modulating Aβ plaque formation.

TABLE 1 Potential amyloid beta (Aβ) 40 and/or Aβ42 interactors selected for validation.

Protein name	Protein ID	Interactor	Ratio Aβ40/Scrambled	Ratio Aβ42/Scrambled
CDC42	P60953	Aβ42	0.7	8.61
CLDN11	O75508	Aβ42	1.18	8.14
CNRIP1	Q96F85	Aβ42	0.96	1.54
CSTB	P04080	Aβ42	0.76	–
FSCN1	Q16658	Aβ42	1.18	1.82
PA2G4	Q9UQ80	Aβ42	1.18	1.61
PRNP	P04156	Aβ42	0.98	1.67
PSMC4	P43686	Aβ42	–	–
PSD3	Q9NYI0	Aβ40	1.96	0.86
PCCA	P05165	Aβ42/Aβ40	2.23	15.02
NRGN	Q92686	Aβ42	1.69	–
PCCB	P05166	Aβ42/Aβ40	2.07	20.44
RHOA	P61586	Aβ42	1.05	2.76
PRKCG	P05129	Aβ40	3.99	1.26
DNM1	Q05193	Aβ40	1.71	0.70
SV2A	Q7L0J3	Aβ42	1.06	1.60

3.4 | Analysis of dysregulation of candidate Aβ interactors in AD

To investigate whether these validated Aβ interactors might be associated with the progression of AD, we next examined whether these proteins were dysregulated in the disease by (1) ICC analysis of established cellular models of AD, (2) WB and IHC analysis of brain tissue samples from AD patients and healthy individuals, and (3) in silico analysis of previous proteomics data using brain tissue samples from patients and controls.

First, hNS1 cells overexpressing APP were used as a model of AD in their proliferative or differentiated states (Figure 4). This neural model, based on APP-stimulated proliferation and differentiation of neural stem cells,[34,35] suggests that proteins dysregulated in this system might be involved in AD-associated Aβ pathology. Notably, PSD3, PRKCG, SV2A, PCCA, PCCB, FSCN1, NRGN, CSTB, CNRIP1, and CLDN11 showed a significant dysregulation during the proliferation state and PSD3, PRKCG, SV2A, PCCA, PCCB, PA2G4, CDC42, CSTB, CNRIP1, and CLDN11 during differentiation, suggesting a role in AD pathology (Figure 4B). In both cases, PRKCG was identified as being downregulated in the disease, whereas the other dysregulated proteins were found to be upregulated upon APP overexpression (Figure 4A,B).

To investigate the dysregulation of these proteins in patients, their protein levels were analyzed by WB in frozen left prefrontal cortex tissue samples from patients at Braak IV–VI and healthy individuals as controls (Figure 5A,B). A statistically significant upregulation was observed for DNM1, PSMC4, PA2G4, PRNP, and CSTB in AD patients, in contrast to healthy individuals, whereas FSCN1 was found to be significantly downregulated in the disease (Figure 5A,B). In addition, some of these proteins were observed to be dysregulated at different stages of the disease (Figure S5a). DNM1, PSD3, and PRKCG were found to be upregulated at Braak IV, whereas their protein levels decreased with the progression of the disease. Moreover, FSCN1 levels were observed to be downregulated at Braak IV and V. PCCA, PSMC4, PA2G4, and PRNP showed a gradual upregulation with the progression of the disease, with statistically significant higher protein levels at advanced Braak V or Braak VI AD stages. In contrast, RHOA showed a progressive downregulation in parallel with the progression of the disease, with significantly lower protein levels at Braak VI. Finally, CSTB was found to be significantly upregulated across all Braak stages, whereas PCCB exhibited slightly elevated levels in the disease. In addition, the downregulation of PRKCG and upregulation of NRGN in AD were previously demonstrated by proteomics, IF, WB, or IHC.[42,45–47]

Furthermore, we performed an in silico analysis using previous proteomics data from AD patients' and controls' brain tissue.[41,42] In a previous TMT analysis performed on the same brain region from AD patients (Braak stages IV–VI) and healthy controls,[42] five of the 16 candidate proteins were found to be dysregulated in AD patients compared to healthy individuals (Figure 5C). Specifically, NRGN and PA2G4 were found to be upregulated (AD/Healthy ratio $\geq$ 1.2) at Braak VI and Braak V, respectively, whereas PSD3, DNM1, and PRKCG were found to be downregulated (AD/Healthy ratio $\leq$ 0.6) at Braak V and VI. Additionally, in a second large-scale TMT proteomics study of the frontal cortex region, encompassing late-stage AD patients with high plaque and tangle pathology (AD, $n = 18$), patients with MCI and high Aβ pathology but mild cognitive deficits (MCI, $n = 18$), individuals with low plaque and tangle pathology (LPC, $n = 18$), and those with high Aβ pathology but no detectable cognitive impairment (HPC, $n = 18$) were found to have significant upregulation for SV2A in the MCI stage, compared to LPC individuals, and significant upregulation of CLDN11 in the MCI stage compared to HPC individuals (Figure 5D).

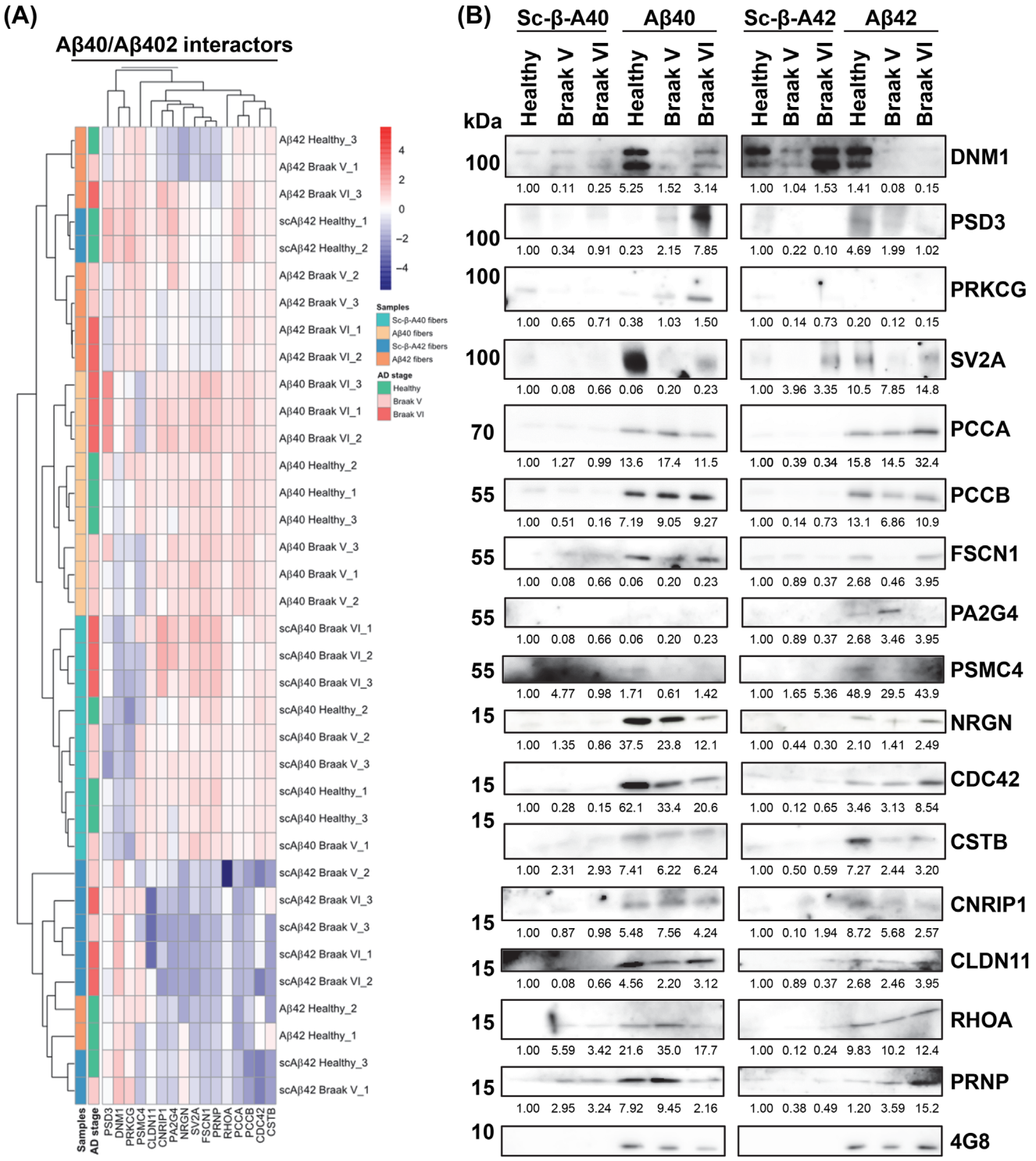

FIGURE 3 Validation of Aβ fiber-interacting proteins. (A) Heatmap of candidate interacting proteins selected for validation clustering according to pathological state and Aβ fibers induced. Log_2 of label-free quantitative relative intensity is represented after row data normalization. (B) Western blot analysis of pull-down replicates with Aβ40 and Aβ42 fibers and protein extracts from Alzheimer's disease patients (Braak V-VI) and healthy individuals confirmed the in vitro interaction of indicated proteins with Aβ peptides. 4G8 immunostaining was used as loading control in pull-down assays. Aβ, amyloid beta.

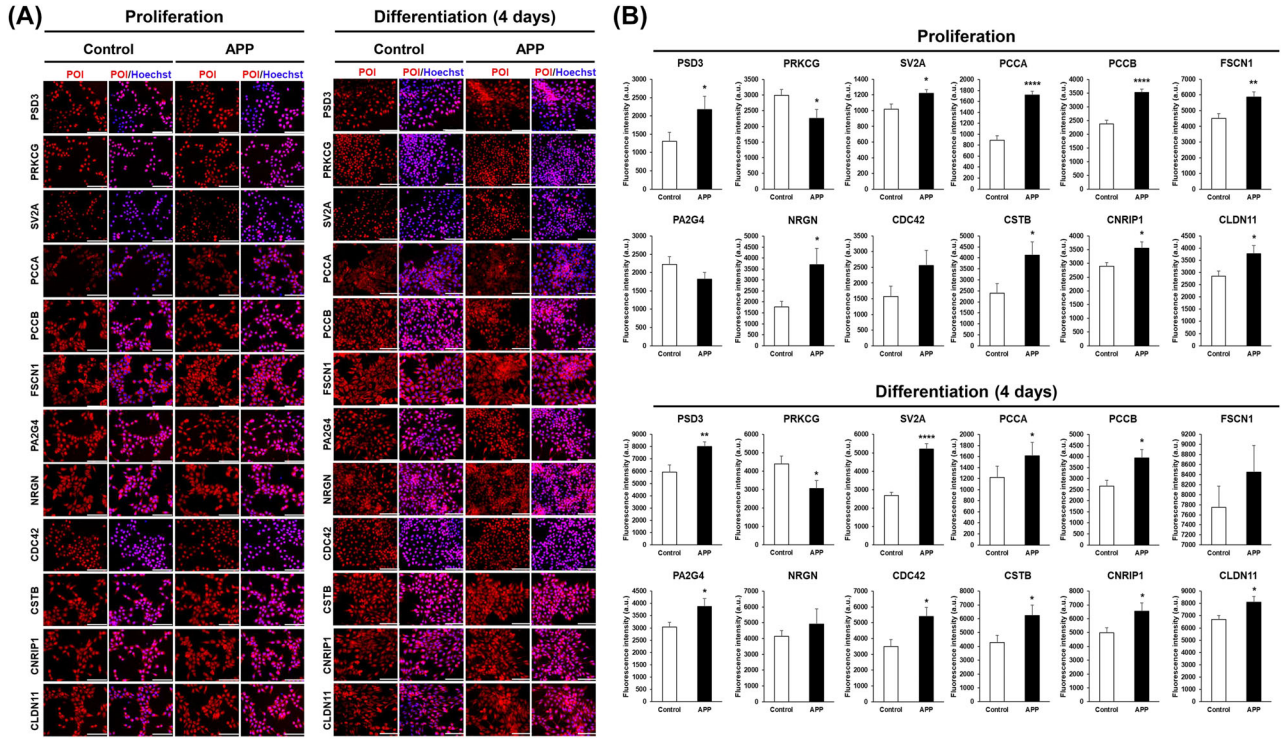

FIGURE 4 In vitro analysis of dysregulation of candidate proteins in hNSI model of AD. (A) Immunofluorescence analysis of PSD3, PRKCG, SV2A, PCCA, PCCB, FSCN1, PA2G4, NRGN, CDC42, CSTB, CNRIP1, and CLDN11 in control hNS1 cells (control) and (APP) overexpressing hNS1 cells APP at proliferation (left) and differentiation (right) conditions. Scale bar: 100 µm. (B) Mean fluorescence intensity and SEM obtained for APP and control cells in proliferation is represented. All proteins but PA2G4 and CDC42 showed a statistically significant dysregulation in AD. (C) Mean fluorescence intensity and SEM obtained for APP and control cells at 4 days of differentiation is represented. All proteins but FSCN1 and NRGN showed a statistically significant dysregulation in AD. *$p < 0.05$; **$p < 0.01$; ****$p < 0.0001$. AD, Alzheimer's disease; APP, amyloid precursor protein; SEM, standard error of the mean.

In contrast, CLDN11 protein levels were diminished in AD patients compared to LPC individuals. These results suggest that the observed dysregulation may be specific to the brain region analyzed. Finally, we also investigated whether any of the validated candidate interactors were differentially secreted into the CSF of AD patients compared to healthy individuals (Figure 5D). Significantly increased levels of PA2G4 were found in AD patients compared to healthy individuals, whereas the release of PCCB, PCCA, SV2A, and DNM1 to CSF was diminished in AD patients, suggesting that the accumulation of Aβ interactors in amyloid plaques primarily reduces their secretion into the CSF and, consequently, into the bloodstream.

To further confirm the dysregulation of these proteins in AD, we performed an IHC analysis using a TMA with FFPE tissue samples from healthy individuals and AD patients at Braak stages IV to VI,[42,45] where neuronal and neuropil staining was investigated. In neurons, a significant downregulation was observed for PSD3 in AD patients, whereas PCCA and PRNP were found to be upregulated in the disease (Figure 6A,B). Additionally, PSD3 was found to be significantly downregulated at Braak IV, V, and VI, whereas higher protein levels of PCCA, PRNP, and PSMC4 were observed at different Braak stages. Furthermore, PCCB and CDC42 were found to be significantly upregulated at Braak IV in comparison to healthy individuals (Figure S5b). Regarding neuropil staining, significantly higher protein levels were found for PCCA and PCCB in AD patients compared to healthy individuals, which were observed to be upregulated at all Braak stages (Figure 6A,C and Figure S5C). Interestingly, PA2G4 neuropil levels were also upregulated in AD patients at different Braak stages (Figure S5c).

3.5 | Association of Aβ interactors to Aβ aggregates *ex vivo*

Finally, to further confirm *ex vivo* the interaction of candidate proteins with Aβ plaques, IF through PLA assay was performed using FFPE tissue samples (Figure 7).

Accumulations of PCCB, PRKCG, CSTB, and PRNP proteins could be observed in Aβ plaques in AD tissue samples (Figure 7A), confirming the role of these proteins as novel Aβ plaque interactors. Additionally, the presence of PRKCG and PCCB in Aβ plaques from healthy individuals was also investigated by PLA. Interestingly, a reduced number of diffuse plaques without accumulation of previously identified interacting proteins was observed in healthy tissue samples (Figure 7B).

This finding highlights the specificity of these novel proteins for plaques associated with AD and underscores the distinct composition of Aβ plaques depending on whether they are related to aging or to the

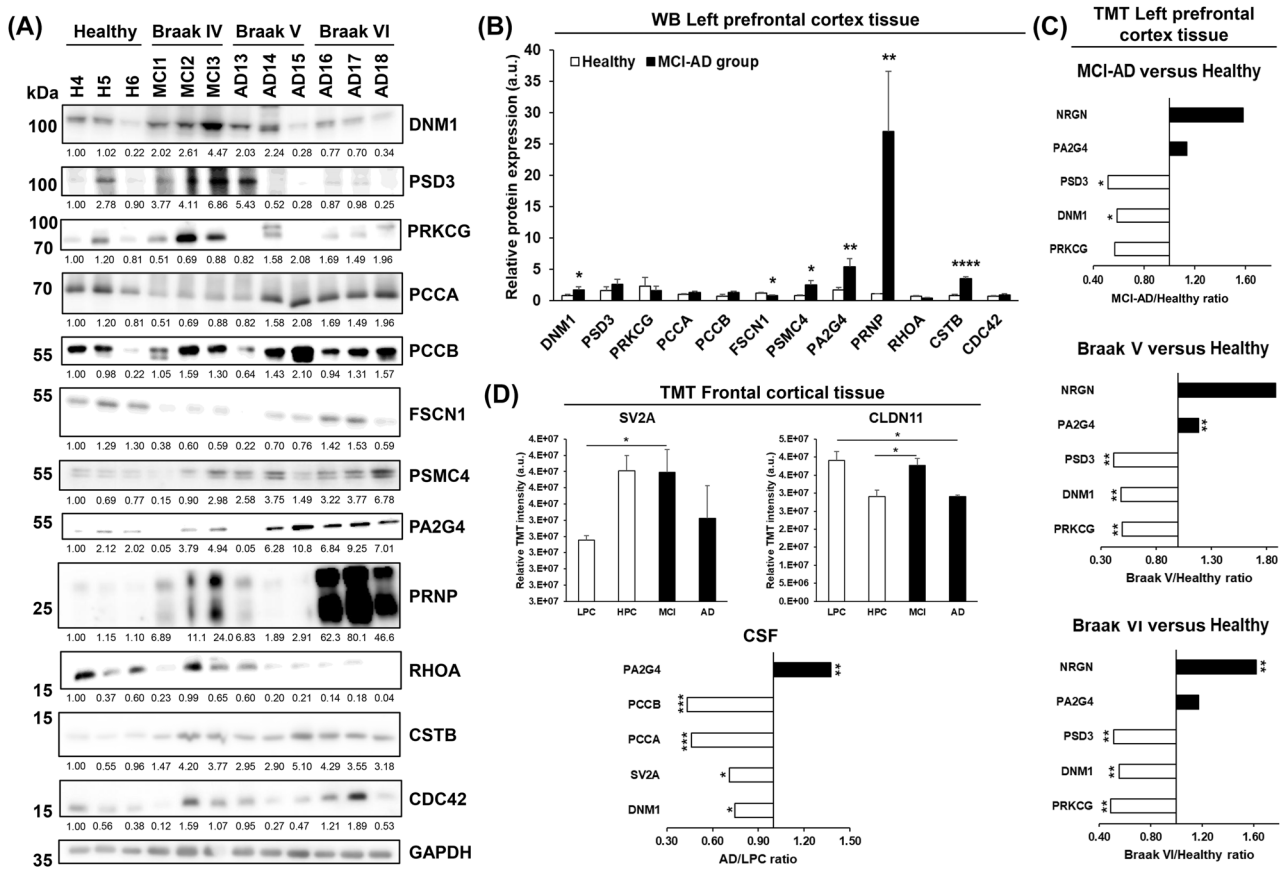

FIGURE 5 In vitro and in silico analysis of dysregulation of selected proteins in brain tissue samples of AD patients and healthy individuals. (A) Western blot analysis of frozen left prefrontal cortex brain tissue samples of AD patients at Braak stages IV, V, and VI and healthy individuals (H). GAPDH was as a loading control and for normalization. (B) Mean protein band intensity and SEM obtained for the healthy and AD samples by WB after data normalization is represented. A statistically significant dysregulation was observed for DNM1, FSCN1, PSMC4, PRNP, and CSTB in AD. Protein band intensities were quantified by densitometry with ImageJ software and normalized according to GAPDH staining. (C) Dysregulation ratio and significance obtained for validated Aβ interactors from a previous TMT analysis using left prefrontal brain tissue samples from AD patients and healthy individuals.[42] Relative TMT protein intensity from all AD samples, AD samples at Braak V, and AD samples at Braak VI were compared to the relative TMT protein intensity from healthy individuals. NRGN, PA2G4, PSD3, DNM1, and PRKCG were confirmed to be dysregulated in the disease. (D) Mean relative TMT protein intensity in frontal cortical tissue from LPC, HPC, MCI, and AD individuals and the SEM is represented. Only SV2A and CLDN11 showed significantly higher protein levels in MCI patients in comparison to controls. In addition, the dysregulation ratio and significance obtained for the validated Aβ interactors from a previous proteomics analysis of the CSF from AD patients and LPC individuals is represented. Release to the CSF of PA2G4, PCCB, PCCA, SV2A, and DNM1 was found to be dysregulated in the disease. $^{*}p < 0.05$; $^{**}p < 0.01$; $^{***}p < 0.001$; $^{****}p < 0.0001$. Aβ, amyloid beta; AD, Alzheimer's disease; CSF, cerebrospinal fluid; MCI, mild cognitive impairment; LPC, low pathology control; HPC, high pathology control; SEM, standard error of the mean; TMT, tandem mass tag; WB, western blot.

disease. Moreover, since PRKCG showed the closest physical proximity or functional association with Aβ aggregates, these results, together with the fact that PRKCG is an enzymatically active kinase previously associated with synaptic plasticity and neurodegeneration,[48–50] would suggest that PRKCG may exert a modulatory effect on fibril formation, particularly during early or seeding stages.

3.6 | Amyloid fibril formation in response to PRKCG modulators measured by high-content confocal imaging

To address this question and evaluate the role of PRKCG in modulating amyloid fibril formation, we employed high-content fluorescence microscopy (Operetta) using CRANAD-2 dye to monitor Aβ40 fibrillization. Human neural stem cells (hNS1) were incubated with 1 μM of the PRKCG activator TPPB or 50 nM of the PRKCG inhibitor PKC-IN-1 (PKCIN1) for 1 h at 37°C and 5% CO_2. An equivalent volume of DMSO was used in control cells. Following treatment, cells were lysed with RIPA buffer, and 2 mg of total protein from each condition were incubated with 10 μM Aβ40 peptide over a time course ranging from 6 h to 24 h. Then 2 μL of each reaction mixture was immobilized on poly-L-lysine-coated 384-well plates, and amyloid fibril formation was quantified through automated image analysis of CRANAD-2 signal, assessing the area, and the perimeter of the amyloid aggregates induced by each PRKCG condition (Figure 7C). Strikingly, aggregates formed when using the PRKCG inhibitor (PKCIN1) were significantly smaller than the aggregates induced with the PRKCG activator (TPPB)

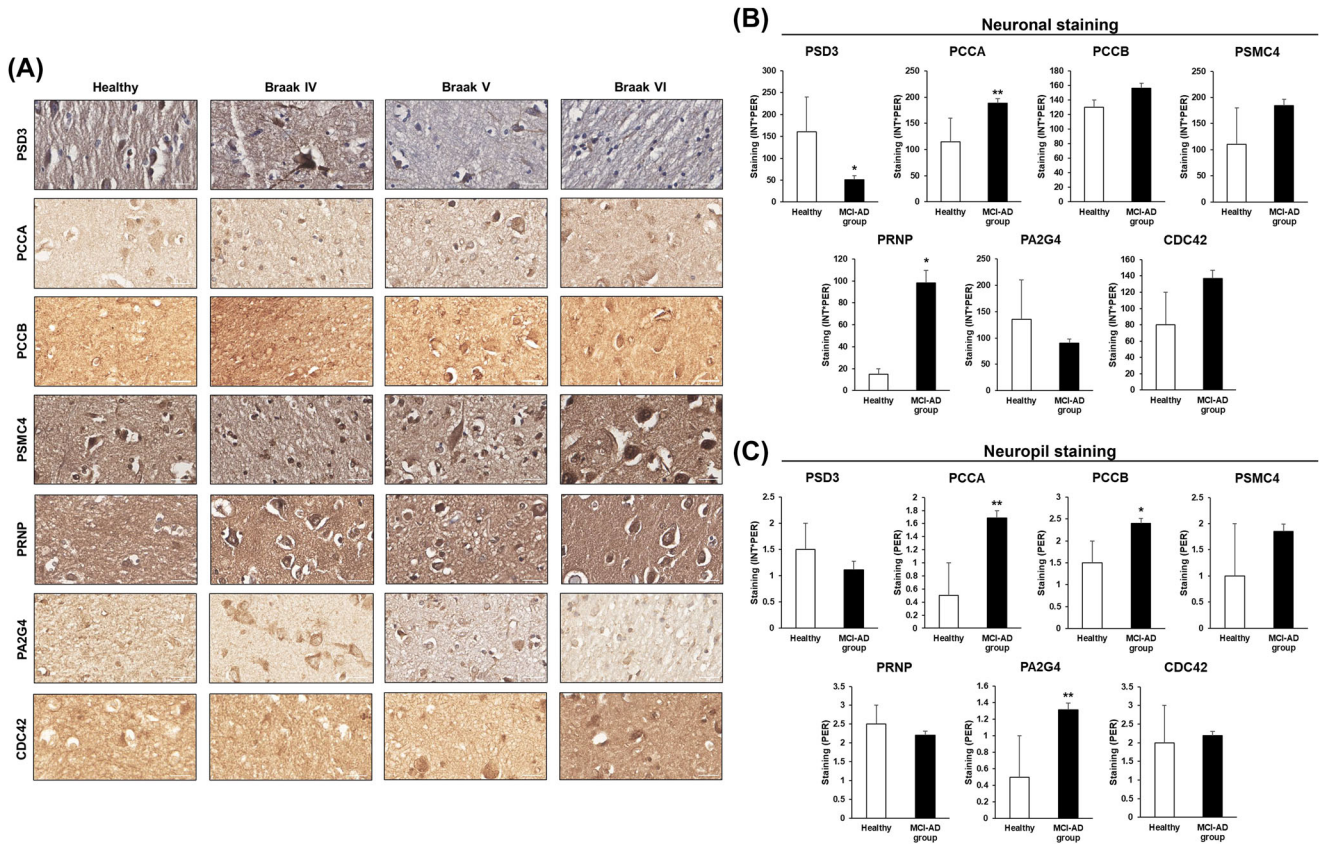

FIGURE 6 TMA and IHC of FFPE left prefrontal tissue samples of AD patients and healthy individuals. (A) Representative 80× magnification images for staining of left prefrontal cortex core of healthy individuals and AD patients with specific antibodies against PSD3, PCCA, PCCB, PSMC4, PRNP, PA2G4, and CDC42. Scale bar: 25 μm. Mean and standard error of the mean (SEM) of total staining intensity (INT*PER) obtained from AD patients and healthy individuals' tissue samples used in TMA and IHC in (B) neurons and in (C) neuropil. The significant dysregulation for PSD3, PCCA, and PRNP in neurons and the significant dysregulation of PCCA, PCCB, and PA2G4 in the neuropil were confirmed. $^{*}p < 0.05$; $^{**}p < 0.01$. AD, Alzheimer's disease; INT, intensity; PER, percentage. AD, Alzheimer's disease; IHC, immunohistochemistry; TMA, tissue microarray.

protein extracts, in terms of area and parameter (Figure 7C,D). Additionally, the Aβ aggregates formed under control conditions (DMSO) and with PRKCG inhibition were morphologically more similar to each other than to those induced by PRKCG activation. Furthermore, we observed a higher number of small aggregates with the control and inhibitor, in contrast to the PRKCG activator, whereas a higher number of large aggregates (>15 μm^2 and >25 μm^2) were observed when the PRKCG activator was used (Figure 7E).

These findings support a functional role of PRKCG in regulating Aβ aggregation, with the PRKCG inhibitor attenuating fibril formation and the PRKCG activator enhancing it. Collectively, these results indicate that modulation of PRKCG activity can significantly impact the kinetics and extent of Aβ fibril formation, suggesting not only a functional role of PRKCG in modulating the amyloidogenic processes but also that AD-related post-translational modifications of PRKCG may promote its selective association with Aβ. Moreover, given the kinase activity of PRKCG and our results (Figures 3 and 7), we propose that pathological phosphorylation of PRKCG in AD facilitates its interaction with Aβ peptides at the membrane surface, promoting early aggregation events and the formation of extracellular Aβ deposits. As fibrillization progresses, Aβ assemblies would sequester PRKCG within maturing plaques, leading to conformational inhibition and a subsequent loss of catalytic activity. This model could also explain the reduced PRKCG levels observed in AD tissues, as its incorporation into insoluble Aβ aggregates would likely decrease its solubility and recovery in biochemical analyses. Altogether, our findings support a bidirectional relationship between PRKCG dysregulation and Aβ aggregation, in which aberrant kinase signaling both contributes to and is exacerbated by amyloid pathology in AD.

4 | DISCUSSION

The aggregation and deposition of Aβ fibrils into plaques throughout the brain begins years before the onset of the first cognitive symptoms of AD. Both soluble and insoluble Aβ species contribute to disease progression, triggering blood–brain barrier dysfunction, disrupted signaling, tau hyperphosphorylation, inflammation, and oxidative stress, ultimately driving neuronal death, neurotransmitter deficits, cognitive decline, and neurodegeneration.[51] Anti-Aβ immunotherapies can transiently reduce plaque burden and delay symptoms, but their efficacy

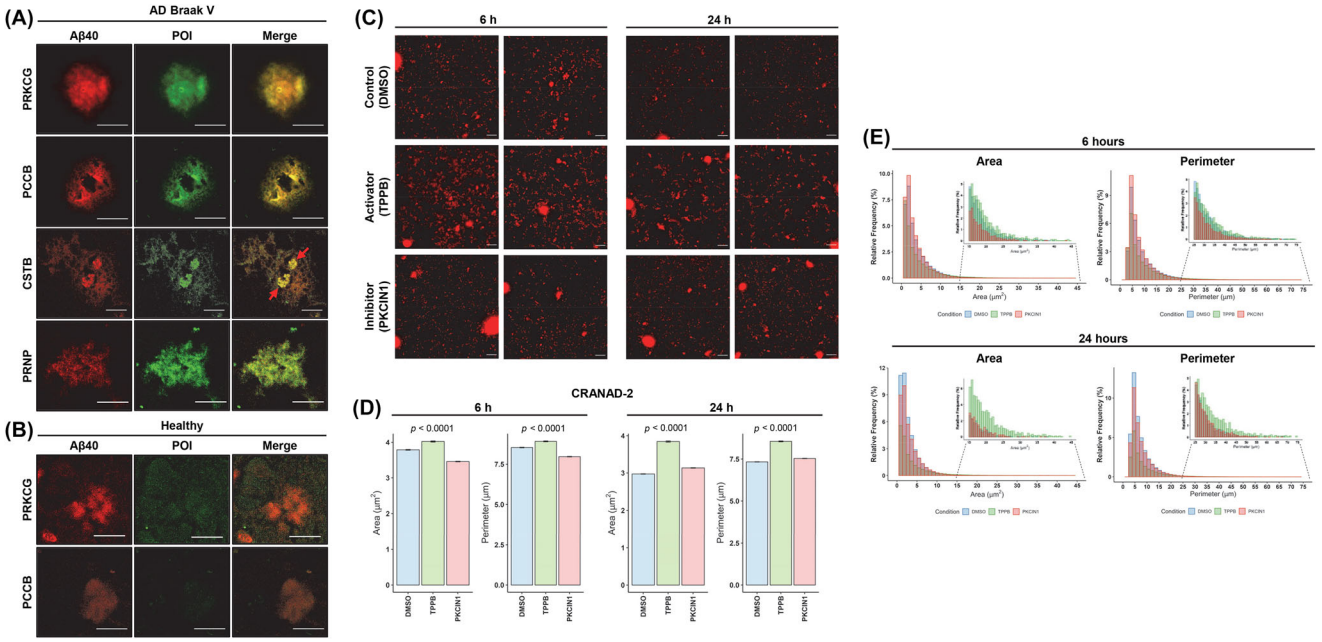

FIGURE 7 PLA analysis validated *ex vivo* Aβ interactors. (A) IF staining with an Aβ40 antibody and an antibody against the protein of interest (POI) confirmed the *ex vivo* interaction between Aβ plaques and PRKCG, PCCB, CSTB, and PRNP in Alzheimer's disease (AD) patients Aβ plaques. Red arrows highlight the presence of autofluorescence due to Lipofuscin aggregates. Scale bar: 10 μm. (B) Immunofluorescence staining with an Aβ40 antibody and an antibody against PCCB or PRKCG confirmed the absence of these proteins in Aβ plaques non-related to AD but to the natural aging of individuals. Scale bar: 10 μm. Signal intensities for Aβ40, PRKCG, and PCCB channels were enhanced in healthy samples in comparison to AD samples, as a lower signal was obtained in the healthy ones. (C–E) High-content fluorescence imaging of Aβ fibril formation in response to PRKCG modulators. (C) Two representative images of indicated conditions after 6 and 24 h of incubation with Aβ40 peptide and protein extracts from hNS1 cells incubated with DMSO (control), TPPB (PRKCG activator), or PKCIN1 (PRKCG inhibitor) are shown. Scale bar: 20 μm. **d)** Bar plot of the mean ± SEM of area and perimeter of control aggregates and aggregates induced with hNS1 cells incubated with PRKCG activator or inhibitor after 6 and 24 h of incubation. (E) Frequency plot of area and perimeter distribution of Aβ40 aggregates induced by different PRKCG modulators. Inset: zoomed-in image of higher area range (15 to 45 μm^2) and perimeter range (25 to 75 μm). The PRKCG inhibitor induced the formation of a higher number of small aggregates, whereas PRKCG activation induced larger aggregates. Aβ, amyloid beta; PLA, proximity ligation assay.

diminishes over time, likely due to plaque heterogeneity and broader neuropathological context.[52]

Two predominant Aβ plaques have been identified in the brain of AD patients, largely composed of protofibrils and typically not linked to neuronal damage and dense-core plaques with a compact fibrillar center surrounded by dystrophic neurites, astrocytes, and microglia.[53,54] In addition to Aβ peptides, plaques contain proteins and cellular components that shape their structure and toxicity.[12] Microglia promote plaque compaction by recruiting toxic oligomers, and Aβ-binding proteins can accelerate fibril aggregation. Since diffuse plaques also occur in aged but cognitively normal individuals, the protein composition of plaques in AD may hold specific pathogenic clues. Thus, proteins identified as Aβ interactors in AD patients may be specifically associated with AD pathology.

Recent proteomics studies focused on characterizing Aβ plaque-associated proteomes in AD patients. These analyses, conducted on LCM plaques and non-plaque FFPE brain tissue sections, have revealed over 100 Aβ plaque-associated proteins,[55] including ARL8B, SMOC1, EZR, MSN, GFAP, and MDK.[21–24] However, LCM and FFPE limit resolution due to protein crosslinking and contamination from adjacent tissue, hindering precise identification of Aβ-specific interactors and reducing the depth of proteome analysis.

To overcome these limitations, we focused on identifying proteins interacting with Aβ40 and Aβ42 fibrils using in vitro synthesized fibrils and protein extracts from the left prefrontal cortex of AD patients and healthy individuals. This was achieved through pull-down assays followed by DDA-LFQ proteomics. The pull-down assays selectively enriched for Aβ-interacting proteins, while proteins not directly associated with Aβ peptides were excluded from the analysis. We also differentiated between proteins interacting with Aβ40 or Aβ42 or with both Aβ species, which may be potentially informed about targeted immunotherapy based on the predominant Aβ plaque composition. Here, we utilized tissue samples rather than cellular models to ensure that the entire brain microenvironment involved in Aβ pathology in AD patients was represented.[12] Tissue samples from Braak stages V and VI AD patients were utilized to maximize detection of Aβ-associated proteins. In parallel, protein extracts from healthy individuals were included to identify Aβ-interacting proteins potentially downregulated in AD patients, while providing a baseline for identifying AD-specific dysregulation. Additionally, pooled tissue samples were used to iden-

tify dominant Aβ-interacting proteins that may drive Aβ pathology in AD, while individual samples were employed for *ex vivo* validation of Aβ interactors.

To identify candidate interactors, we first performed a dysregulation analysis in which proteins with a fold change ≥1.5 and a FDR ≤0.05 in Aβ samples (healthy, Braak V, Braak VI) versus Scrambled controls were selected (Scrambled analysis). This approach identified 85 potential interactors: five common to both Aβ40 and Aβ42, 17 specific to Aβ40, and 63 specific to Aβ42. To expand coverage, we conducted a complementary specificity analysis, selecting proteins uniquely detected in Aβ samples but absent in Scrambled controls. This dual strategy addressed the limitations of proteomics studies: Dysregulation analysis highlighted proteins with quantitative abundance differences, including those present at lower levels in controls, whereas specificity analysis captured proteins with strong exclusive Aβ interactions, even if not meeting strict fold-change/FDR criteria. By combining both analyses, we broadened the net of potential interactors, increasing the likelihood of detecting novel Aβ-binding proteins and building a more complete map of the Aβ interactome. Importantly, Aβ samples from healthy individuals were not considered true controls, given the >90% correlation in brain protein content between AD and non-AD tissue, as most Aβ interactors are present in both cohorts. Nevertheless, we confirmed that some proteins identified here, while detectable in healthy tissue, did not accumulate in Aβ plaques lacking AD pathology. This distinction underscores their disease relevance, suggesting that specific Aβ interactors may contribute directly to plaque maturation and pathogenicity in AD. Thus, to further assess their role, the contribution of these interactors to Aβ plaque maturation at prodromal (Braak I and II) and MCI (Braak III and IV) stages should be examined to determine their involvement in plaque formation.

Remarkably, several proteins identified here were previously reported as Aβ interactors in other proteomics studies, including APP, PMP2, FGG, and CSTB. Notably, tau (MAPT) was not strongly enriched as an Aβ-associated protein (enrichment ratio 1.2 to 1.3), but it was still significantly upregulated among both Aβ40 and Aβ42 interactors. Other proteins previously described as Aβ-associated were not detected in our analysis, possibly due to differences in the brain regions studied and Aβ plaque distribution and composition.

Bioinformatics revealed enrichment in metabolic pathways, consistent with oxidative stress and mitochondrial dysfunction in AD, and in synaptic proteins, suggesting links to disrupted cell communication and AD progression.[56,57] Additionally, several synaptic proteins were identified as Aβ interactors, suggesting a potential role of those proteins in cell communication and AD progression. 16 candidate proteins were prioritized for validation, favoring Aβ42 interactors, given its predominance in plaques. These included DNM1, SV2A, PRKCG, PA2G4, PSMC4, PSD3, PCCA, PCCB, NRGN, FSCN1, CDC42, CTSB, CNRIP1, CLDN11, RHOA, and PRNP. Validation by WB, immunofluorescence, and PLA confirmed all selected interacting proteins except DNM1, PRKCG, and PA2G4 to interact with both Aβ40 and Aβ42 peptides in Aβ plaques. While our proteomics analysis primarily identified these proteins as Aβ40 or Aβ42 interactors, this observation may be attributed to their enhanced adhesive properties. *Ex vivo* findings provide compelling evidence that novel Aβ interactors specifically accumulate in Aβ plaques associated with AD, but not in those found in healthy individuals, highlighting disease specificity.

This specificity suggests that Aβ plaques in AD differ molecularly from age-related plaques, with interactors potentially contributing to plaque maturation and toxicity. Their selective recruitment points to functional involvement rather than passive deposition, emerging as promising targets to potentially disrupt plaque formation or mitigate its toxic effects.

Interestingly, most of the Aβ-interacting proteins were observed to be dysregulated in AD brain tissue by WB, in silico, and/or IHC and ICC analyses. PCCA, PCCB, PA2G4, CSTB, PSMC4, and NRGN were upregulated, whereas proteins PSD3 and PRKCG were downregulated in the left prefrontal cortex brain tissue of AD patients. This suggests that the recruitment of interacting proteins to plaques by Aβ peptides could either contribute to or result from cellular dysfunction in AD. Additionally, the altered CSF secretion of PA2G4, PCCB, PCCA, SV2A, and DNM1 in AD may reflect plasma biomarker potential.

Among notable interactors previously implicated in neurodegeneration or other diseases, PRNP, which is related to Creutzfeldt–Jakob disease, is involved in neuronal development and synaptic plasticity[58] and known as a cell surface receptor for Aβ oligomers.[59] PSD3, an oncogene linked to thyroid cancer,[60] is highly enriched in the brain, as reported by the Human Protein Atlas, and downregulated at the mRNA level in AD but poorly studied in neurodegeneration.[61] Moreover, PSD3 interaction and expression patterns in AD and control tissues resemble those of PRKCG, suggesting it as another Aβ interactor of interest in AD. DNM1, involved in vesicular transport and endocytosis,[62] has not been previously linked to AD. CTSB is implicated in cancer and lysosomal dysfunction.[63] NRGN, a post-synaptic protein kinase, has been repeatedly shown to be altered in AD.[42,64] PCCB, a mitochondrial enzyme,[65] has emerged as a novel AD interactor.

Finally, PRKCG, a neuron-specific kinase involved in synaptic plasticity, learning, and memory, deserves special attention. Exclusively expressed in the brain and spinal cord, PRKCG is localized to neurons,[48] where its activity sustains long-term potentiation (LTP), a process essential for memory formation.[49,50] PRKCG downregulation has been linked to psychiatric disorders and neurodegeneration, and our data confirm its reduction in AD brain tissue and colocalization with plaques. Functional assays showed that PRKCG activity modulated Aβ fibril morphology: Activation promoted larger fibrils, while inhibition favored smaller aggregates. This dual behavior suggests that chronic PRKCG downregulation could impair LTP and synaptic plasticity, contributing to cognitive decline, while also influencing amyloid aggregation. Thus, PRKCG may act as both a biomarker and a mechanistic link between Aβ pathology and synaptic dysfunction. Importantly, an aberrant PRKCG phosphorylation would not imply a protective role but rather indicate that PRKCG becomes progressively inactivated due to aggregation into Aβ plaques. Indeed, although chronic modulation may inadvertently exacerbate AD risk, our results could allow the hypothesis that PRKCG inhibitors would represent an interesting approach to improving AD symptoms or delaying its progression.

5 | CONCLUSIONS

This study expands the Aβ interactome by identifying and validating novel fibril-binding proteins with diagnostic and therapeutic potential. Many of the proteins identified are dysregulated in AD, and their selective accumulation in pathological plaques highlights their likely functional roles. PRKCG stands out as a key candidate linking amyloidogenesis with synaptic dysfunction, while PCCB, PSD3, and others represent unexplored avenues. These findings reinforce the concept that Aβ plaques in AD are molecularly distinct from age-related plaques and that their interactors could serve as both biomarkers and therapeutic targets.

AUTHOR CONTRIBUTIONS

A.M-C. and R.B.: Conceptualization. A.M-C., R.C., V.R., A.R, A.P-G., I.L., and R.B.: Methodology. A.M-C., R.C., V.R., M.J.F-A., J.M.U, J.M., D.M., and A.P-G.: Investigation. A.M-C. and R.B.: Writing – original draft. A.M-C., R.C., V.R., MJ.F-A., J.M.U, A.R, J.M., D.M., A.P-G., I.L., and R.B.: Writing – review and editing. V.R., I.L., and R.B.: Resources. A.M-C., MJ.F-A., A.P-G., I.L., and R.B.: Supervision. I.L. and R.B.: Funding acquisition. All authors read and approved the manuscript.

ACKNOWLEDGMENTS

We gratefully acknowledge the invaluable technical support provided by the Unidad de Microscopía Electrónica of the Instituto de Salud Carlos III. We acknowledge the financial support of the PMP22/00084 grant of the 2022 personalized medicine call from the Instituto de Salud Carlos III (ISCIII), the PI17CIII/00045 grant from the AES-ISCIII program, and grant PID2022-140307OB-I00 funded by MCIN/AEI/10.13039/501100011033 and by "ERDF A way of making Europe" to R.B.; R.C. and I.L. acknowledge grant PID2021-126715OB-I00 financed by MCIN/AEI/10.13039/501100011033 and "ERDF A way of making Europe" and PI22CIII/00055 funded by the AES-ISCIII program from ISCIII. A.M.-C. was supported by a predoctoral contract of the Fundación Tatiana Pérez de Guzmán El Bueno, followed by a FPU predoctoral supported by the Spanish Ministerio de Educación, Cultura y Deporte and a postdoctoral grant associated with the PMP22/00084 project of ISCIII.

ETHICS APPROVAL AND CONSENT TO PARTICIPATE

The Institutional Ethical Review Board of the Spanish Research Center for Neurological Diseases Foundation (CIEN) and the Instituto de Salud Carlos III approved this study on proteomics analysis and biomarker discovery of Alzheimer's disease (CEI PI 45).

CONFLICT OF INTEREST STATEMENT

The authors declare no competing interests. Author disclosures are available in the Supporting Information.

DATA AVAILABILITY STATEMENT

The data supporting the findings of this study are available in the paper and the Supporting Information. Source data are provided with this paper. The mass spectrometry proteomics data have been deposited at the ProteomeXchange Consortium via the PRIDE partner repository with the dataset identifier PXD061100. Any other relevant data are also available from the corresponding authors upon request.

CONSENT FOR PUBLICATION

All authors of this article gave consent to publish the manuscript.

ORCID

Rodrigo Barderas https://orcid.org/0000-0003-3539-7469

REFERENCES

1. 2020 Alzheimer's disease facts and figures. *Alzheimers Dement*. 2020;16:391-460. doi:10.1002/alz.12068
2. Murphy MP. Alzheimer's disease and the amyloid-beta peptide. *J Alzheimers Dis*. 2010;19(1):311-323. doi:10.3233/JAD-2010-1221
3. Hampel H, Hardy J, Blennow K, et al. The amyloid-beta pathway in Alzheimer's disease. *Mol Psychiatry*. 2021;26:5481-5503. doi:10.1038/s41380-021-01249-0
4. Ono M, Watanabe H, Kitada A, Matsumura K, Ihara M, Saji H. Highly selective Tau-SPECT imaging probes for detection of neurofibrillary tangles in Alzheimer's disease. *Sci Rep*. 2016;6:34197. doi:10.1038/srep34197
5. DeTure MA, Dickson DW. The neuropathological diagnosis of Alzheimer's disease. *Mol Neurodegener*. 2019;14(1):32. doi:10.1186/s13024-019-0333-5
6. Thal DR, Rub U, Orantes M, Braak H. Phases of A beta-deposition in the human brain and its relevance for the development of AD. *Neurology*. 2002;58(12):1791-1800. doi:10.1212/wnl.58.12.1791
7. Walker LC. Abeta Plaques. *Free Neuropathol*. 2020;1:31. doi:10.17879/freeneuropathology-2020-3025
8. Chen GF, Xu TH, Yan Y, et al. Amyloid beta: structure, biology and structure-based therapeutic development. *Acta Pharmacol Sin*. 2017;38(9):1205-1235. doi:10.1038/aps.2017.28
9. Gandy S, Caporaso G, Buxbaum J, Frangione B, Greengard P. APP processing, a beta-amyloidogenesis, and the pathogenesis of Alzheimer's disease. *Neurobiol Aging*. 1994;15(2):253-256. doi:10.1016/0197-4580(94)90125-2
10. Zhang YW, Thompson R, Zhang H, Xu H. APP processing in Alzheimer's disease. *Mol Brain*. 2011;4:3. doi:10.1186/1756-6606-4-3
11. Holtzman DM, Bales KR, Tenkova T, et al. Apolipoprotein E isoform-dependent amyloid deposition and neuritic degeneration in a mouse model of Alzheimer's disease. *Proc Natl Acad Sci U S A*. 2000;97(6):2892-2897. doi:10.1073/pnas.050004797
12. Rahman MM, Lendel C. Extracellular protein components of amyloid plaques and their roles in Alzheimer's disease pathology. *Mol Neurodegener*. 2021;16(1):59. doi:10.1186/s13024-021-00465-0
13. Serrano-Pozo A, Frosch MP, Masliah E, Hyman BT. Neuropathological alterations in Alzheimer disease. *Cold Spring Harb Perspect Med*. 2011;1(1):a006189. doi:10.1101/cshperspect.a006189
14. Finder VH, Glockshuber R. Amyloid-beta aggregation. *Neurodegener Dis*. 2007;4(1):13-27. doi:10.1159/000100355
15. Meinhardt J, Sachse C, Hortschansky P, Grigorieff N, Fandrich M. Abeta(1-40) fibril polymorphism implies diverse interaction patterns in amyloid fibrils. *J Mol Biol*. 2009;386(3):869-877. doi:10.1016/j.jmb.2008.11.005
16. Luhrs T, Ritter C, Adrian M, et al. 3D structure of Alzheimer's amyloid-beta(1-42) fibrils. *Proc Natl Acad Sci U S A*. 2005;102(48):17342-17347. doi:10.1073/pnas.0506723102
17. Haass C, Selkoe DJ. Soluble protein oligomers in neurodegeneration: lessons from the Alzheimer's amyloid beta-peptide. *Nat Rev Mol Cell Biol*. 2007;8(2):101-112. doi:10.1038/nrm2101

18. Rijal Upadhaya A, Capetillo-Zarate E, Kosterin I, et al. Dispersible amyloid beta-protein oligomers, protofibrils, and fibrils represent diffusible but not soluble aggregates: their role in neurodegeneration in amyloid precursor protein (APP) transgenic mice. *Neurobiol Aging*. 2012;33(11):2641-2660. doi:10.1016/j.neurobiolaging.2011.12.032
19. Glabe CG. Structural classification of toxic amyloid oligomers. *J Biol Chem*. 2008;283(44):29639-29643. doi:10.1074/jbc.R800016200
20. Friedrich RP, Tepper K, Ronicke R, et al. Mechanism of amyloid plaque formation suggests an intracellular basis of Abeta pathogenicity. *Proc Natl Acad Sci U S A*. 2010;107(5):1942-1947. doi:10.1073/pnas.0904532106
21. Drummond E, Kavanagh T, Pires G, et al. The amyloid plaque proteome in early onset Alzheimer's disease and down syndrome. *Acta Neuropathol Commun*. 2022;10(1):53. doi:10.1186/s40478-022-01356-1
22. Drummond E, Nayak S, Faustin A, et al. Proteomic differences in amyloid plaques in rapidly progressive and sporadic Alzheimer's disease. *Acta Neuropathol*. 2017;133(6):933-954. doi:10.1007/s00401-017-1691-0
23. Liao L, Cheng D, Wang J, et al. Proteomic characterization of postmortem amyloid plaques isolated by laser capture microdissection. *J Biol Chem*. 2004;279(35):37061-37068. doi:10.1074/jbc.M403672200
24. Xiong F, Ge W, Ma C. Quantitative proteomics reveals distinct composition of amyloid plaques in Alzheimer's disease. *Alzheimers Dement*. 2019;15(3):429-440. doi:10.1016/j.jalz.2018.10.006
25. Friedrich C, Schallenberg S, Kirchner M, et al. Comprehensive micro-scaled proteome and phosphoproteome characterization of archived retrospective cancer repositories. *Nat Commun*. 2021;12(1):3576. doi:10.1038/s41467-021-23855-w
26. Dapic I, Uwugiaren N, Kers J, Mohammed Y, Goodlett DR, Corthals G. Evaluation of fast and sensitive proteome profiling of FF and FFPE kidney patient tissues. *Molecules*. 2022;27(3):1137. doi:10.3390/molecules27031137
27. Davalieva K, Kiprijanovska S, Dimovski A, Rosoklija G, Dwork AJ. Comparative evaluation of two methods for LC-MS/MS proteomic analysis of formalin fixed and paraffin embedded tissues. *J Proteomics*. 2021;235:104117. doi:10.1016/j.jprot.2021.104117
28. Montero-Calle A, Garranzo-Asensio M, Rejas-Gonzalez R, et al. Benefits of FAIMS to improve the proteome coverage of deteriorated and/or cross-linked TMT 10-Plex FFPE tissue and plasma-derived exosomes samples. *Proteomes*. 2023;11(4):35. doi:10.3390/proteomes11040035
29. Martinez-Martin P, Avila J, AD Research Unit Investigators. Alzheimer center reina sofia foundation: fighting the disease and providing overall solutions. *J Alzheimers Dis*. 2010;21(2):337-348. doi:10.3233/JAD-2010-101149
30. Hyman BT, Phelps CH, Beach TG, et al. National institute on aging-Alzheimer's association guidelines for the neuropathologic assessment of Alzheimer's disease. *Alzheimers Dement*. 2012;8(1):1-13. doi:10.1016/j.jalz.2011.10.007
31. Montine TJ, Phelps CH, Beach TG, et al. National institute on aging-Alzheimer's association guidelines for the neuropathologic assessment of Alzheimer's disease: a practical approach. *Acta Neuropathol*. 2012;123(1):1-11. doi:10.1007/s00401-011-0910-3
32. Mirra SS, Hart MN, Terry RD. Making the diagnosis of Alzheimer's disease. A primer for practicing pathologists. *Arch Pathol Lab Med*. 1993;117(2):132-144.
33. Zea-Sevilla MA, Fernandez-Blazquez MA, Calero M, Bermejo-Velasco P, Rabano A. Combined Alzheimer's disease and cerebrovascular staging explains advanced dementia cognition. *Alzheimers Dement*. 2015;11(11):1358-1366. doi:10.1016/j.jalz.2015.01.004
34. Coronel R, Lachgar M, Bernabeu-Zornoza A, et al. Neuronal and glial differentiation of human neural stem cells is regulated by amyloid precursor protein (APP) levels. *Mol Neurobiol*. 2019;56(2):1248-1261. doi:10.1007/s12035-018-1167-9
35. Coronel R, Palmer C, Bernabeu-Zornoza A, et al. Physiological effects of amyloid precursor protein and its derivatives on neural stem cell biology and signaling pathways involved. *Neural Regen Res*. 2019;14(10):1661-1671. doi:10.4103/1673-5374.257511
36. Wisniewski JR, Gaugaz FZ. Fast and sensitive total protein and Peptide assays for proteomic analysis. *Anal Chem*. 2015;87(8):4110-4116. doi:10.1021/ac504689z
37. Torra J, Viela F, Megias D, Sot B, Flors C. Versatile near-infrared super-resolution imaging of amyloid fibrils with the fluorogenic probe CRANAD-2. *Chemistry*. 2022;28(19):e202200026. doi:10.1002/chem.202200026
38. Szklarczyk D, Gable AL, Lyon D, et al. STRING v11: protein-protein association networks with increased coverage, supporting functional discovery in genome-wide experimental datasets. *Nucleic Acids Res*. 2019;47(D1):D607-D613. doi:10.1093/nar/gky1131
39. Huang DW, Sherman BT, Tan Q, et al. DAVID bioinformatics resources: expanded annotation database and novel algorithms to better extract biology from large gene lists. *Nucleic Acids Res*. 2007;35(Web Server issue):W169-W175. doi:10.1093/nar/gkm415
40. Dennis G Jr, Sherman BT, Hosack DA, et al. DAVID: database for annotation, visualization, and integrated discovery. *Genome Biol*. 2003;4(5):P3.
41. Bai B, Wang X, Li Y, et al. Deep multilayer brain proteomics identifies molecular networks in alzheimer's disease progression. *Neuron*. 2020;105(6):975-991 e7. doi:10.1016/j.neuron.2019.12.015
42. Montero-Calle A, Coronel R, Garranzo-Asensio M, et al. Proteomics analysis of prefrontal cortex of Alzheimer's disease patients revealed dysregulated proteins in the disease and novel proteins associated with amyloid-beta pathology. *Cell Mol Life Sci*. 2023;80(6):141. doi:10.1007/s00018-023-04791-y
43. Bardou P, Mariette J, Escudie F, Djemiel C, Klopp C. jvenn: an interactive Venn diagram viewer. *BMC Bioinformatics*. 2014;15:293. doi:10.1186/1471-2105-15-293
44. Inoue Y, Tasaki M, Masuda T, et al. alpha-Enolase reduces cerebrovascular Abeta deposits by protecting Abeta amyloid formation. *Cell Mol Life Sci*. 2022;79(8):462. doi:10.1007/s00018-022-04493-x
45. Garranzo-Asensio M, San Segundo-Acosta P, Martinez-Useros J, et al. Identification of prefrontal cortex protein alterations in Alzheimer's disease. *Oncotarget*. 2018;9(13):10847-10867. 10.18632/oncotarget.24303
46. Begcevic I, Kosanam H, Martinez-Morillo E, et al. Semiquantitative proteomic analysis of human hippocampal tissues from Alzheimer's disease and age-matched control brains. *Clin Proteomics*. 2013;10(1):5. doi:10.1186/1559-0275-10-5
47. Andreev VP, Petyuk VA, Brewer HM, et al. Label-free quantitative LC-MS proteomics of Alzheimer's disease and normally aged human brains. *J Proteome Res*. 2012;11(6):3053-3067. doi:10.1021/pr3001546
48. Saito N, Shirai Y. Protein kinase C gamma (PKC gamma): function of neuron specific isotype. *J Biochem*. 2002;132(5):683-687. doi:10.1093/oxfordjournals.jbchem.a003274
49. Grados M, Salehi M, Lotfi A, Dua S, Xie I. A selective review of inhibitors of protein kinase C gamma: a neuroplasticity-related common pathway for psychiatric illness. *Front Drug Deliv*. 2024;4:1364037. doi:10.3389/fddev.2024.1364037
50. Chopra R, Wasserman AH, Pulst SM, De Zeeuw CI, Shakkottai VG. Protein kinase C activity is a protective modifier of Purkinje neuron degeneration in cerebellar ataxia. *Hum Mol Genet*. 2018;27(8):1396-1410. doi:10.1093/hmg/ddy050
51. Lane CA, Hardy J, Schott JM. Alzheimer's disease. *Eur J Neurol*. 2018;25(1):59-70. doi:10.1111/ene.13439

52. Song C, Shi J, Zhang P, et al. Immunotherapy for Alzheimer's disease: targeting beta-amyloid and beyond. *Transl Neurodegener*. 2022;11(1):18. doi:10.1186/s40035-022-00292-3
53. Sheng JG, Mrak RE, Griffin WS. Neuritic plaque evolution in Alzheimer's disease is accompanied by transition of activated microglia from primed to enlarged to phagocytic forms. *Acta Neuropathol*. 1997;94(1):1-5. doi:10.1007/s004010050664
54. Lemke G, Huang Y. The dense-core plaques of Alzheimer's disease are granulomas. *J Exp Med*. 2022;219(8):e20212477. doi:10.1084/jem.20212477
55. Drummond ES, Nayak S, Ueberheide B, Wisniewski T. Proteomic analysis of neurons microdissected from formalin-fixed, paraffin-embedded Alzheimer's disease brain tissue. *Sci Rep*. 2015;5:15456. doi:10.1038/srep15456
56. Cheignon C, Tomas M, Bonnefont-Rousselot D, Faller P, Hureau C, Collin F. Oxidative stress and the amyloid beta peptide in Alzheimer's disease. *Redox Biol*. 2018;14:450-464. doi:10.1016/j.redox.2017.10.014
57. Abramov AY, Canevari L, Duchen MR. Beta-amyloid peptides induce mitochondrial dysfunction and oxidative stress in astrocytes and death of neurons through activation of NADPH oxidase. *J Neurosci*. 2004;24(2):565-575. doi:10.1523/JNEUROSCI.4042-03.2004
58. Ladogana A, Kovacs GG. Genetic Creutzfeldt-Jakob disease. *Handb Clin Neurol*. 2018;153:219-242. doi:10.1016/B978-0-444-63945-5.00013-1
59. Zhou J, Liu B. Alzheimer's disease and prion protein. *Intractable Rare Dis Res*. 2013;2(2):35-44. doi:10.5582/irdr.2013.v2.2.35
60. Jin L, Zheng D, Bhandari A, et al. PSD3 is an oncogene that promotes proliferation, migration, invasion, and G1/S transition while inhibits apoptotic in papillary thyroid cancer. *J Cancer*. 2021;12(18):5413-5422. doi:10.7150/jca.60885
61. Quan X, Liang H, Chen Y, Qin Q, Wei Y, Liang Z. Related network and differential expression analyses identify nuclear genes and pathways in the hippocampus of Alzheimer disease. *Med Sci Monit*. 2020;26:e919311. doi:10.12659/MSM.919311
62. Gammie AE, Kurihara LJ, Vallee RB, Rose MD. DNM1, a dynamin-related gene, participates in endosomal trafficking in yeast. *J Cell Biol*. 1995;130(3):553-566. doi:10.1083/jcb.130.3.553
63. Zhu W, Dong X, Luo S, Guo S, Zhou W, Song W. Transcriptional activation of CSTB gene expression by transcription factor Sp3. *Biochem Biophys Res Commun*. 2023;649:71-78. doi:10.1016/j.bbrc.2023.01.087
64. Sun X, Wang Q, Blennow K, et al. Association of neurogranin gene expression with Alzheimer's disease pathology in the perirhinal cortex. *Alzheimers Dement (N Y)*. 2021;7(1):e12162. doi:10.1002/trc2.12162
65. Wongkittichote P, Ah Mew N, Chapman KA. Propionyl-CoA carboxylase—A review. *Mol Genet Metab*. 2017;122(4):145-152. doi:10.1016/j.ymgme.2017.10.002

SUPPORTING INFORMATION

Additional supporting information can be found online in the Supporting Information section at the end of this article.

How to cite this article: Montero-Calle A, Coronel R, Manosalva J, et al. Comprehensive profiling of Aβ40 and Aβ42 fibril-interacting proteins reveals PRKCG as a drug-targetable regulator of amyloidogenesis in Alzheimer's disease. *Alzheimer's Dement*. 2026;22:e71090. https://doi.org/10.1002/alz.71090